RADIATIVE TRANSFER: A NEW LOOK OF THE OLD THEORY

Michael I. Mishchenko

NASA Goddard Institute for Space Studies, 2880 Broadway,
New York, NY 10025, USA

ABSTRACT. This tutorial paper discusses electromagnetic scattering by random many-particle groups and summarizes the microphysical approach to radiative transfer and coherent backscattering. It provides a detailed discussion of the exact meaning of such fundamental concepts as single and multiple scattering and explains how the theories of radiative transfer and coherent backscattering originate in the macroscopic Maxwell equations. It also exposes and corrects certain misconceptions of the traditional phenomenological approach to radiative transfer.

1. INTRODUCTION

Since its inception in the late 19th century [1, 2], the theory of electromagnetic energy transfer in macroscopic media composed of sparsely and randomly distributed, elastically scattering particles has had an enormously rich history of practical applications in numerous areas of science, medicine, and engineering [3–19]. At the same time, it has also had a remarkably rich history of confusing and even misleading accounts of its fundamental principles. The palette of phenomenological derivations of the radiative transfer equation (RTE) encountered in various monographs, textbooks, and reviews is quite diverse, which by itself is a sign of a serious problem. On one hand, most of the derivations are rather short and either present the RTE as a trivial consequence of energy conservation or expect the reader to accept the RTE as a fundamental experimental law implicitly supplementing other basic physical principles such as the laws of classical and quantum electrodynamics. On the other hand, there are derivations which rise to the level of a philosophical essay in which the RTE emerges as an allegedly logical outcome of a multi-page discourse almost devoid of formulas but full of ill-defined collective effects, elementary volume elements, and incoherent light rays. Some of the derivations even invoke the concept of photons as localized particles of light, discrete blobs of energy without phases, or corpuscles that are moving according to the laws of classical mechanics. As such, they imply that the notorious wave–particle duality of light somehow manifests itself in the scattering process that is fully controlled by the macroscopic Maxwell equations.

The use of the "photonic" language in application to elastically scattering, macroscopic particulate media is especially inaccurate and misleading. Indeed, we are asked to accept that light propagates as a stream of photons between the particles, decides to become a wave when it impinges upon a particle and thereby generates a multitude of spectacular effects such as diffraction, glory, morphology-dependent resonances, etc., and then changes its mind again upon leaving the particle and resumes its journey in the form of photons. The physical insolvency of this juggling with waves and photons is obvious. First of all, it is the process of interaction of light with matter that may require quantization of energy, not the process of light propagation. Second, photons appear as the result of quantization of the electromagnetic field. Therefore, whatever is called a "photon" in order to derive the RTE remains an imaginary object with no physical meaning unless the electromagnetic field is quantized explicitly. Needless to say, the latter is never done. Third, it takes opening a standard textbook on quantum electrodynamics or quantum optics (e.g., [20–23]) to realize that a photon is a quantum of a single normal mode of the electromagnetic field and as such is associated with a plane wave of definite wave vector but infinite lateral extent. Therefore, photons are not localized particles of light [24, 25] and cannot be used to define quantities such as the specific intensity or the specific intensity column vector

In: M. P. Mengüç and N. Selçuk, Eds. (2007) *Radiative Transfer–V*, Begell House, New York, pp. 1–30.

[26]. Fourth, it is well established, albeit now widely publicized, that the alleged particle behavior of light in phenomena such as the photoelectric and Compton effects is explainable in terms of the semi-classical approach wherein the electromagnetic field is not quantized and is described by the classical Maxwell equations [24, 25, 27, 28]. One of the pioneers of lasers and misers Charles H. Townes remarked in 1984 that "physicists were somewhat diverted by an emphasis in the world of physics on the photon properties of light rather than its coherent aspects" [29]. This remark remains quite topical.

However realistic the various phenomenological accounts of radiative transfer (RT) may look at first sight, they inevitably fall apart upon scrutiny of their physical foundation. It is, therefore, not surprising that as recently as in 1995, Mandel and Wolf [22] stated that "in spite of the extensive use of the theory of radiative energy transfer, no satisfactory derivation of its basic equation from electromagnetic theory has been obtained up to now." Furthermore, the phenomenological accounts completely overlook the fundamental link between radiative transfer and the effect of coherent backscattering (CB). Most importantly, they conceal the irrefutable fact that as long as scattering occurs without frequency redistribution and the particles are macroscopic and can be characterized by a refractive index, the RTE describes multiple scattering of classical electromagnetic waves and, as such, must be derived directly from the macroscopic Maxwell equations via a series of well defined and reproducible analytical steps [30, 31].

This uncomfortable situation has finally changed, and a complete derivation of the RTE directly from the Maxwell equations for the case of elastically scattering discrete random media has been published [32–34]. This derivation can be used to clarify the role and physical meaning of the various quantities entering the RTE, establish a direct link between the theories of RT and CB, cross-examine the terminologies used in the traditional phenomenological and the new microphysical approaches, and identify and correct certain misconceptions of the phenomenological approach. These are the four main objectives of this tutorial paper. My goal here is not to replace the monograph [34] but rather to provide a brief yet coherent outline which could convince the reader that the microphysical approach to RT is both necessary and feasible.

2. BASIC ASSUMPTIONS

The derivation of the RTE for elastically scattering, random particulate media rests on the following basic assumptions.

1. At each moment in time, the entire scattering object (e.g., a cloud of water droplets or a powder surface) can be represented by a specific spatial configuration of a number N of discrete finite particles (Fig. 1). The unbounded host medium surrounding the scattering object is homogeneous, linear, isotropic, and nonabsorbing. Each particle is sufficiently large so that it can be characterized by constitutive parameters appropriate to bulk matter. Electromagnetically, the presence of a particle means that the constitutive parameters inside the particle volume are different from those of the surrounding host medium.

2. The scattering object is illuminated by either:

   (i) a plane electromagnetic wave given by

$$\begin{cases} \mathbf{E}^{\rm inc}(\mathbf{r},t) = \mathbf{E}_0^{\rm inc}\exp(\mathrm{i}\mathbf{k}^{\rm inc}\cdot\mathbf{r} - \mathrm{i}\omega t), \\ \mathbf{H}^{\rm inc}(\mathbf{r},t) = \mathbf{H}_0^{\rm inc}\exp(\mathrm{i}\mathbf{k}^{\rm inc}\cdot\mathbf{r} - \mathrm{i}\omega t), \end{cases} \qquad \mathbf{r}\in\Re^3 \tag{1}$$

   with constant amplitudes $\mathbf{E}_0^{\rm inc}$ and $\mathbf{H}_0^{\rm inc}$, where $\mathbf{E}$ is the electric and $\mathbf{H}$ the magnetic field, ω is the angular frequency, $\mathbf{k}^{\rm inc}$ is the real-valued wave vector, $\mathbf{r}$ is the position (radius) vector, $\mathrm{i} = (-1)^{1/2}$, and $\Re^3$ denotes the entire three-dimensional space; or

   (ii) a quasi-monochromatic parallel beam of light given by

$$\begin{cases} \mathbf{E}^{\rm inc}(\mathbf{r},t) = \mathbf{E}_0^{\rm inc}(t)\exp(\mathrm{i}\mathbf{k}^{\rm inc}\cdot\mathbf{r} - \mathrm{i}\omega t), \\ \mathbf{H}^{\rm inc}(\mathbf{r},t) = \mathbf{H}_0^{\rm inc}(t)\exp(\mathrm{i}\mathbf{k}^{\rm inc}\cdot\mathbf{r} - \mathrm{i}\omega t), \end{cases} \qquad \mathbf{r}\in\Re^3, \tag{2}$$

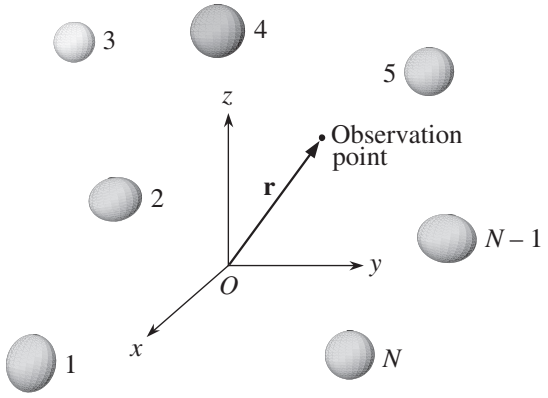

Figure 1. Scattering object in the form of a group of N discrete particles.

where fluctuations in time of the complex amplitudes of the electric and magnetic fields, $\mathbf{E}_0^{\text{inc}}(t)$ and $\mathbf{H}_0^{\text{inc}}(t)$, around their respective mean values occur much more slowly than the harmonic oscillations of the time factor $\exp(-\mathrm{i}\omega t)$.

This restriction excludes other types of illumination such as a focused laser beam of finite lateral extent or a pulsed beam.

3. Nonlinear optics effects are excluded by assuming that the constitutive parameters of both the scattering object and the surrounding medium are independent of the electric and magnetic fields.
4. It is assumed that electromagnetic scattering occurs without frequency redistribution, i.e., the scattered light has the same frequency as the incident light. This restriction excludes inelastic scattering phenomena and the specific consideration of the small Doppler shift of frequency of the scattered light relative to that of the incident light due the movement of the particles with respect to the source of illumination.
5. It is assumed that any significant changes in the scattering object (e.g., changes in particle positions and/or orientations with respect to the laboratory reference frame) occur over time intervals T much longer than the period of time-harmonic oscillations of the electromagnetic field: $T \gg 2\pi/\omega$.
6. The phenomenon of thermal emission is excluded. This assumption is usually valid for objects at room or lower temperature and for short-wave infrared and shorter wavelengths.

3. THE MACROSCOPIC MAXWELL EQUATIONS

The assumptions listed in the preceding section imply that all fields and sources are time harmonic and allow one to fully describe the total electromagnetic field at any moment in time everywhere in space as the solution of the frequency-domain macroscopic differential Maxwell equations [35, 36]. The specific dependence of the constitutive parameters on spatial coordinates and the corresponding boundary conditions at any moment are fully defined by the instantaneous geometrical configuration of the N particles (Fig. 1).

The frequency-domain Maxwell equations yield the magnetic field provided that the electric field is known everywhere. Therefore, the solution of these equations is usually sought in terms of only the electric field.

4. ELECTROMAGNETIC SCATTERING

The term “electromagnetic scattering” has been used in the preceding sections without a prior strict definition. We will now fill this gap.

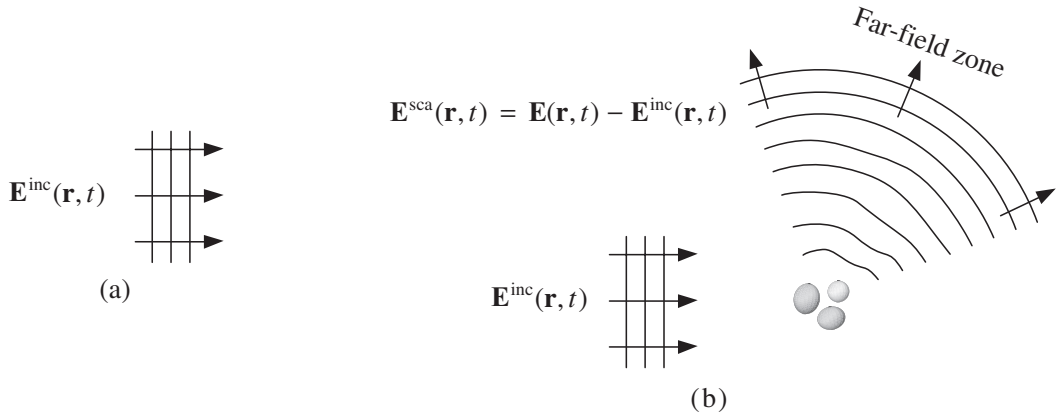

Figure 2. Scattering by a fixed finite object. In this case the object consists of three disjoint, stationary particles.

It is well known that the Maxwell equations allow for a fundamental solution in the form of a time-harmonic plane electromagnetic wave [35, 36]. This solution represents the transport of electromagnetic energy from one point to another and embodies the concept of a perfectly monochromatic parallel beam of light. A plane electromagnetic wave propagates in an infinite nonabsorbing medium without a change in its intensity or polarization state (see Fig. 2(a)). However, the presence of a finite object modifies both the electric and the magnetic field that would otherwise exist in an unbounded homogeneous space. This modification is called *electromagnetic scattering*.

The difference between the total field in the presence of the object, $\mathbf{E}(\mathbf{r},t)$, and the original field that would exist in the absence of the object, $\mathbf{E}^{\mathrm{inc}}(\mathbf{r},t)$, can be thought of as the field scattered by the object, $\mathbf{E}^{\mathrm{sca}}(\mathbf{r},t)$ (Fig. 2(b)). In other words, the total field in the presence of the object is represented as the vector sum of the respective incident (original) and scattered fields:

$$\mathbf{E}(\mathbf{r},t) = \mathbf{E}^{\mathrm{inc}}(\mathbf{r},t) + \mathbf{E}^{\mathrm{sca}}(\mathbf{r},t). \tag{3}$$

The reader should recognize that the separation of the total field into the incident and scattered fields according to Eq. (3) is a purely mathematical procedure. This means that classical electromagnetic scattering is not a physical process per se but rather an abbreviated way to state that the total field computed in the presence of an object is different from that computed in the absence of the object. To "describe electromagnetic scattering" then means to quantify the difference between the two fields as a function of the object physical properties.

To appreciate this fundamental point, let us recall that a plane electromagnetic wave is a stationary solution of the Maxwell equations in that it is assumed to have existed for ever and, apart from the time-harmonic factor $\exp(-\mathrm{i}\omega t)$, with no temporal change. The solution of the frequency-domain Maxwell equations in the presence of the scattering object is also stationary. This implies that the scattered field is also stationary since it is defined mathematically as the difference between two stationary fields. Therefore, classical electromagnetic scattering is not a temporally discrete event and cannot be visualized, for example, in terms of a light ray (or a localized blob of energy) approaching the object, then being scattered, and then propagating in an outward direction.

In practice, the applicability of the frequency-domain formalism implies the stationarity of the electromagnetic field over a time interval long compared with the period of time-harmonic oscillations. Therefore, this formalism can be used to describe scattering of quasi-monochromatic as well as monochromatic light.

An especially transparent description of electromagnetic scattering is afforded by the so-called volume integral equation (VIE) which follows from the frequency-domain macroscopic Maxwell equations and is exact [37, 38]:

$$\mathbf{E}(\mathbf{r}) = \mathbf{E}^{\rm inc}(\mathbf{r}) + k_1^2 \int_{V_{\rm INT}} {\rm d}\mathbf{r}' \vec{G}(\mathbf{r},\mathbf{r}') \cdot \mathbf{E}(\mathbf{r}') [m^2(\mathbf{r}') - 1]$$

$$= \mathbf{E}^{\rm inc}(\mathbf{r}) + k_1^2 \left(\vec{I} + \frac{1}{k_1^2} \nabla \otimes \nabla \right) \cdot \int_{V_{\rm INT}} {\rm d}\mathbf{r}' \, \mathbf{E}(\mathbf{r}') \frac{\exp({\rm i}k_1|\mathbf{r} - \mathbf{r}'|)}{4\pi|\mathbf{r} - \mathbf{r}'|} [m^2(\mathbf{r}') - 1], \quad \mathbf{r} \in \Re^3, \quad (4)$$

where the common factor $\exp(-{\rm i}\omega t)$ is omitted, $V_{\rm INT}$ is the cumulative "interior" volume occupied by the scattering object, $m(\mathbf{r}')$ is the refractive index of the interior relative to that of the host exterior medium, $k_1 = |\mathbf{k}^{\rm inc}|$ is the wave number in the host medium, $\vec{G}(\mathbf{r},\mathbf{r}')$ is the free space dyadic Green's function, $\vec{I}$ is the identity dyadic, and $\otimes$ is the dyadic product sign. One can see that the VIE expresses the total field everywhere in space in terms of the total internal field. If the scattering object is absent, $m(\mathbf{r}') \equiv 1$, then the total field is identically equal to the incident field. Otherwise the total field contains a scattering component given by the second term on the right-hand side of Eq. (4). Since the internal field is not known in general, it must be found by solving the VIE either analytically or numerically.

The VIE makes explicit two fundamental facts. First, the phenomenon of electromagnetic scattering is not limited to the case of the incident field in the form of a plane electromagnetic wave. In fact, it encompasses any incident field as long as the latter satisfies the Maxwell equations, e.g., spherical and cylindrical electromagnetic waves.

Second, irrespective of the morphological structure of the scattering object the latter remains a single, unified scatterer. Although the human eye may classify the scattering object as a "collection of discrete particles", the incident field always perceives the object as one scatterer in the form of the specific spatial distribution of the relative refractive index.

The latter point can be made even more explicit by expressing the scattered electric field in terms of the incident field:

$$\mathbf{E}^{\rm sca}(\mathbf{r}) = \int_{V_{\rm INT}} {\rm d}\mathbf{r}' \vec{G}(\mathbf{r},\mathbf{r}') \cdot \int_{V_{\rm INT}} {\rm d}\mathbf{r}'' \vec{T}(\mathbf{r}',\mathbf{r}'') \cdot \mathbf{E}^{\rm inc}(\mathbf{r}''), \quad \mathbf{r} \in \Re^3, \quad (5)$$

where $\vec{T}$ is the so-called dyadic transition operator of the scattering object [39]. Substituting Eq. (5) in Eq. (4) yields the following integral equation for $\vec{T}$:

$$\vec{T}(\mathbf{r},\mathbf{r}') = k_1^2 [m^2(\mathbf{r}) - 1] \delta(\mathbf{r} - \mathbf{r}') \vec{I}$$

$$+ k_1^2 [m^2(\mathbf{r}) - 1] \int_{V_{\rm INT}} {\rm d}\mathbf{r}'' \vec{G}(\mathbf{r},\mathbf{r}'') \cdot \vec{T}(\mathbf{r}'',\mathbf{r}'), \quad \mathbf{r},\mathbf{r}' \in V_{\rm INT}, \quad (6)$$

where $\delta(\mathbf{r})$ is the three-dimensional delta function. Equations of this type appear in the quantum theory of scattering and are called Lippmann–Schwinger equations [40]. The advantage of Eqs. (5) and (6) is that $\vec{T}$ is the property of the scattering object only and is independent of the incident field. Furthermore, $\vec{T}$ provides a complete description of electromagnetic scattering by the object for any incident field. We will see later that the concept of dyadic transition operator plays a central role in the theory of multiple scattering.

The ubiquitous presence of electromagnetic scattering in natural and artificial environments explains its fundamental importance in accurate modeling of electromagnetic energy transport for various science and engineering applications. This also applies to situations in which electromagnetic scattering is induced artificially and used for particle characterization purposes. The exact theoretical and numerical techniques for the computation of the electromagnetic field elastically scattered by a finite fixed object composed of one or several particles are many and are reviewed thoroughly in [38, 41–44]. Unfortunately, all of these techniques have certain practical limitations in terms of the object morphology and object size relative to the incident wavelength and cannot be used yet to describe electromagnetic scattering by large multi-particle objects such as atmospheric clouds, particulate surfaces, and particle suspensions. This makes imperative the use of well-characterized approximate solutions that do not require unrealistic computer resources while being sufficiently

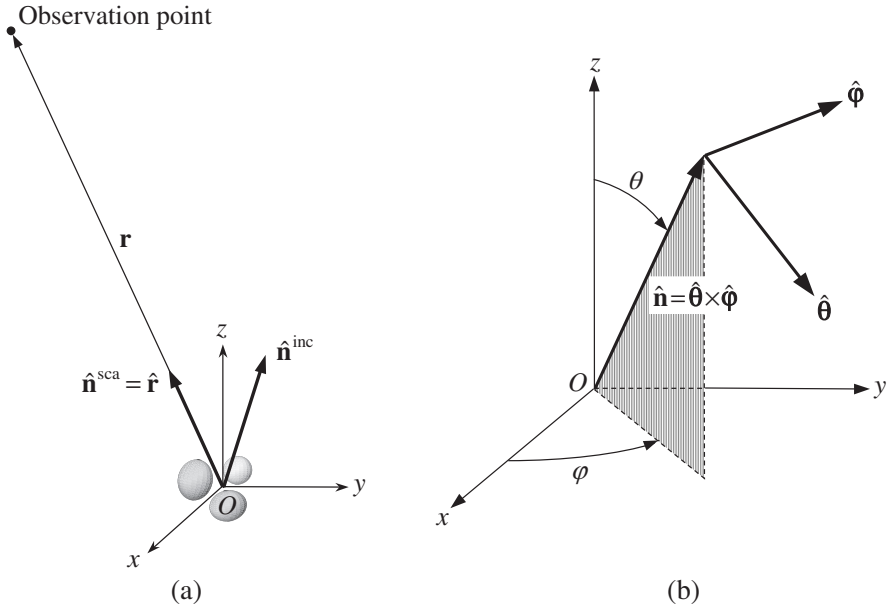

Figure 3. (a) Scattering in the far-field zone of the entire object. (b) Right-handed spherical coordinate system.

accurate for specific applications. One of the main objectives of this paper is to demonstrate that the microphysical theories of RT and CB are two such useful approximations.

5. FAR-FIELD AND NEAR-FIELD SCATTERING

A fundamental property of the dyadic Green's function is the following asymptotic behavior:

$$\vec{G}(\mathbf{r},\mathbf{r}') \underset{r\to\infty}{\to} (\vec{I}-\hat{\mathbf{r}}\otimes\hat{\mathbf{r}})\frac{\exp(\mathrm{i}k_1 r)}{4\pi r}\exp(-\mathrm{i}k_1\hat{\mathbf{r}}\cdot\mathbf{r}'), \tag{7}$$

where $r=|\mathbf{r}|$, and $\hat{\mathbf{r}}=\mathbf{r}/r$. Placing the origin of the laboratory coordinate system O close to the geometrical center of the scattering object and substituting Eqs. (1) and (7) in Eq. (5) yields [34, 38]

$$\mathbf{E}^{\rm sca}(\hat{\mathbf{r}}) \underset{r\to\infty}{\to} \frac{\exp(\mathrm{i}k_1 r)}{r}\mathbf{E}_1^{\rm sca}(r\hat{\mathbf{n}}^{\rm sca}) = \frac{\exp(\mathrm{i}k_1 r)}{r}\vec{A}(\hat{\mathbf{n}}^{\rm sca},\hat{\mathbf{n}}^{\rm inc})\cdot\mathbf{E}_0^{\rm inc}, \qquad \hat{\mathbf{n}}^{\rm sca}\cdot\mathbf{E}_1^{\rm sca}(r\hat{\mathbf{n}}^{\rm sca}) = 0, \tag{8}$$

where $\hat{\mathbf{n}}^{\rm inc}=\mathbf{k}^{\rm inc}/k_1$ is a unit vector in the incidence direction, $\hat{\mathbf{n}}^{\rm sca}=\hat{\mathbf{r}}$ is a unit vector in the scattering direction, Fig. 3(a), and $\vec{A}$ is the so-called scattering dyadic such that

$$\hat{\mathbf{n}}^{\rm sca}\cdot\vec{A}(\hat{\mathbf{n}}^{\rm sca},\hat{\mathbf{n}}^{\rm inc}) = \mathbf{0}, \qquad \vec{A}(\hat{\mathbf{n}}^{\rm sca},\hat{\mathbf{n}}^{\rm inc})\cdot\hat{\mathbf{n}}^{\rm inc} = \mathbf{0}. \tag{9}$$

The scattering dyadic has the dimension of length and describes the scattering of a plane electromagnetic wave in the so-called *far-field zone*. It follows from Eqs. (8) and (9) that the propagation of the scattered electromagnetic wave is away from the object. Furthermore, the electric and magnetic field vectors vibrate in the plane perpendicular to the propagation direction and their amplitudes decay inversely with distance from the object.

The main convenience of the far-field approximation is that it allows one to treat the entire object essentially as a point source of scattered radiation and reduces the scattered field to a simple outgoing spherical wave, Fig. 2(b). Furthermore, Eq. (9) shows that only four out of the nine components of the scattering dyadic are independent in the spherical polar coordinate system centered at the origin, Fig. 3(a). It is therefore convenient to introduce the 2×2 so-called amplitude scattering matrix $\mathbf{S}$, which describes the transformation of the θ- and φ-components of the incident

plane wave into the θ- and φ-components of the scattered spherical wave:

$$\mathbf{E}^{\mathrm{sca}}(r\hat{\mathbf{n}}^{\mathrm{sca}}) = \frac{\exp(\mathrm{i}k_1 r)}{r}\mathbf{S}(\hat{\mathbf{n}}^{\mathrm{sca}}, \hat{\mathbf{n}}^{\mathrm{inc}})\mathbf{E}_0^{\mathrm{inc}}. \tag{10}$$

Here $\mathbf{E}$ denotes a two-component column formed by the θ- and φ-components of the electric field vector:

$$\mathbf{E} = \begin{bmatrix} E_\theta \\ E_\varphi \end{bmatrix}, \tag{11}$$

$\theta \in [0, \pi]$ is the polar (zenith) angle measured from the positive z-axis, and $\varphi \in [0, 2\pi)$ is the azimuth angle measured from the positive x-axis in the clockwise direction when looking in the direction of the positive z-axis, Fig. 3(b). The amplitude scattering matrix has the dimension of length and depends on the incidence and scattering directions as well as on the size, morphology, composition, and orientation of the scattering object with respect to the coordinate system. It also depends on the choice of the origin of the coordinate system relative to the object. If known, the amplitude scattering matrix yields the scattered and thus the total field, thereby providing a complete description of the scattering pattern in the far-field zone.

The conditions defining the far-field zone are as follows [34]:

$$k_1(r - a) \gg 1, \tag{12}$$

$$r \gg a, \tag{13}$$

$$r \gg \frac{k_1 a^2}{2}, \tag{14}$$

where a is the radius of the smallest circumscribing sphere of the entire scattering object centered at O. These conditions are often satisfied for sufficiently small ($k_1 a \lesssim 10^4$) isolated single-particle scatterers. The exact or approximate computation of the amplitude scattering matrix for such particles from the Maxwell equations is also often possible, which explains the widespread use of the amplitude scattering matrix as a single-particle electromagnetic characteristic.

However, there are many important cases in which the conditions (12)–(14) are grossly violated. A good example is remote sensing of water clouds in the terrestrial atmosphere using detectors of electromagnetic radiation mounted on aircraft or satellite platforms. Such detectors typically measure radiation coming from a small part of a cloud and do not "perceive" the entire cloud as a single point-like scatterer (detector 1 in Fig. 4). Furthermore, the notion of the far-field zone of the cloud becomes completely meaningless if a detector is placed inside the cloud (detector 2). It is thus clear that to model theoretically the response of these detectors one has to use scattering characteristics other than the scattering dyadic or the amplitude scattering matrix.

6. ACTUAL OBSERVABLES

Because of high frequency of time-harmonic oscillations, traditional optical instruments cannot measure the electric and magnetic fields associated with the incident and scattered waves. Indeed, accumulating and averaging a signal proportional to the electric or the magnetic field over a time interval T long compared with the period of oscillations would yield a zero net result:

$$\frac{1}{T}\int_t^{t+T} \mathrm{d}t' \exp(-\mathrm{i}\omega t') \underset{T \gg 2\pi/\omega}{=} 0. \tag{15}$$

Therefore, the majority of optical instruments measure quantities which have the dimension of energy flux and are defined in such a way that the time-harmonic factor $\exp(-\mathrm{i}\omega t)$ vanishes upon multiplication by its complex-conjugate counterpart: $\exp(-\mathrm{i}\omega t)[\exp(-\mathrm{i}\omega t)]^* \equiv 1$. This means that

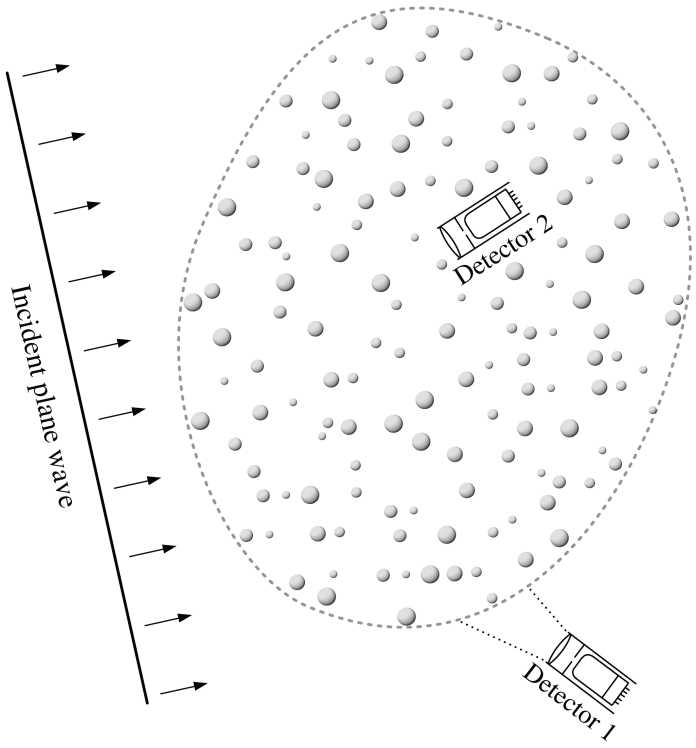

Figure 4. Near-field scattering by a multi-particle group.

in order to make the theory applicable to analyses of actual optical observations, the scattering process must be characterized in terms of carefully chosen derivative quantities that can be measured directly. This explains why the concept of an actual *observable* is central to the discipline of light scattering by particles.

Although one can always define the magnitude and the direction of the electromagnetic energy flux at any point in space in terms of the Poynting vector, the latter carries no information about the polarization state of the incident and scattered fields. The conventional approach to ameliorate this problem dates back to Stokes [45]. He proposed using four real-valued quantities, I, Q, U, and V, which have the dimension of monochromatic energy flux (Wm^{-2}) and fully characterize a *transverse* electromagnetic wave[1] inasmuch as it is subject to practical optical analysis. These quantities, called the Stokes parameters, form the so-called four-component Stokes column vector $\mathbf{I}$ and carry information about both the total intensity, I, and the polarization state of the wave.

In the case of far-field scattering, the tranversality of both the incident plane wave and the scattered spherical wave allows one to define the corresponding sets of Stokes parameters:

$$\mathbf{I}^{\mathrm{inc}} = \begin{bmatrix} I^{\mathrm{inc}} \\ Q^{\mathrm{inc}} \\ U^{\mathrm{inc}} \\ V^{\mathrm{inc}} \end{bmatrix} = \frac{1}{2}\sqrt{\frac{\epsilon_1}{\mu_0}} \begin{bmatrix} E_{0\theta}^{\mathrm{inc}}(E_{0\theta}^{\mathrm{inc}})^* + E_{0\varphi}^{\mathrm{inc}}(E_{0\varphi}^{\mathrm{inc}})^* \\ E_{0\theta}^{\mathrm{inc}}(E_{0\theta}^{\mathrm{inc}})^* - E_{0\varphi}^{\mathrm{inc}}(E_{0\varphi}^{\mathrm{inc}})^* \\ -E_{0\theta}^{\mathrm{inc}}(E_{0\varphi}^{\mathrm{inc}})^* - E_{0\varphi}^{\mathrm{inc}}(E_{0\theta}^{\mathrm{inc}})^* \\ \mathrm{i}[E_{0\varphi}^{\mathrm{inc}}(E_{0\theta}^{\mathrm{inc}})^* - E_{0\theta}^{\mathrm{inc}}(E_{0\varphi}^{\mathrm{inc}})^*] \end{bmatrix}, \tag{16}$$

$$\mathbf{I}^{\mathrm{sca}}(r\hat{\mathbf{n}}^{\mathrm{sca}}) = \begin{bmatrix} I^{\mathrm{sca}} \\ Q^{\mathrm{sca}} \\ U^{\mathrm{sca}} \\ V^{\mathrm{sca}} \end{bmatrix} = \frac{1}{r^2}\frac{1}{2}\sqrt{\frac{\epsilon_1}{\mu_0}} \begin{bmatrix} E_{1\theta}^{\mathrm{sca}}(E_{1\theta}^{\mathrm{sca}})^* + E_{1\varphi}^{\mathrm{sca}}(E_{1\varphi}^{\mathrm{sca}})^* \\ E_{1\theta}^{\mathrm{sca}}(E_{1\theta}^{\mathrm{sca}})^* - E_{1\varphi}^{\mathrm{sca}}(E_{1\varphi}^{\mathrm{sca}})^* \\ -E_{1\theta}^{\mathrm{sca}}(E_{1\varphi}^{\mathrm{sca}})^* - E_{1\varphi}^{\mathrm{sca}}(E_{1\theta}^{\mathrm{sca}})^* \\ \mathrm{i}[E_{1\varphi}^{\mathrm{sca}}(E_{1\theta}^{\mathrm{sca}})^* - E_{1\theta}^{\mathrm{sca}}(E_{1\varphi}^{\mathrm{sca}})^*] \end{bmatrix}, \tag{17}$$

[1] By definition, the electric and magnetic field vectors of a transverse electromagnetic wave vibrate in the plane perpendicular to the propagation direction.

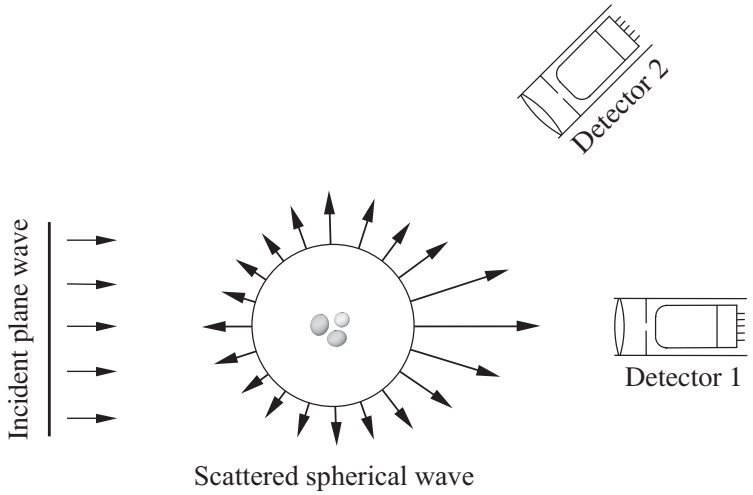

Figure 5. Definition of the extinction and phase matrices.

where ϵ_1 is the electric permittivity of the host medium and μ_0 is the permeability of a vacuum (the scattering object and the host medium are both assumed to be nonmagnetic). Then the response of a well-collimated polarization-sensitive detector of light can be described in terms of the 4×4 so-called phase and extinction matrices.

Specifically, detector 2 in Fig. 5 collects only the scattered light, and its response is fully characterized by the product of the phase matrix $\mathbf{Z}$ and the Stokes column vector of the incident wave:

$$\textbf{Signal 2} = \Delta S\,\mathbf{I}^{\rm sca}(r\hat{\mathbf{n}}^{\rm sca}) = \frac{\Delta S}{r^2}\mathbf{Z}(\hat{\mathbf{n}}^{\rm sca},\hat{\mathbf{n}}^{\rm inc})\mathbf{I}^{\rm inc}, \qquad \hat{\mathbf{n}}^{\rm sca}\neq\hat{\mathbf{n}}^{\rm inc}, \tag{18}$$

where ΔS is the area of the sensitive surface of the detector. Thus the phase matrix realizes the transformation of the Stokes parameters of the incident wave into the Stokes parameters of the scattered wave. The elements of the phase matrix have the dimension of area and are quadratic combinations of the elements of the amplitude scattering matrix $\mathbf{S}(\hat{\mathbf{n}}^{\rm sca},\hat{\mathbf{n}}^{\rm inc})$.

The response of detector 1 facing the incident light consists of three parts:

1. the one due to the incident light;
2. the one due to the forward-scattered light; and
3. the one due to the interference of the incident wave and the wave scattered by the object in the exact forward direction:

$$\begin{aligned}\textbf{Signal 1} &= \int_{\Delta S} {\rm d}S\,\mathbf{I}(r\hat{\mathbf{r}})\\ &= \Delta S\,\mathbf{I}^{\rm inc} + \frac{\Delta S}{r^2}\mathbf{Z}(\hat{\mathbf{n}}^{\rm inc},\hat{\mathbf{n}}^{\rm inc})\mathbf{I}^{\rm inc} - \mathbf{K}(\hat{\mathbf{n}}^{\rm inc})\mathbf{I}^{\rm inc} \qquad (19a)\\ &= \Delta S\,\mathbf{I}^{\rm inc} + \boldsymbol{O}(r^{-2}) - \mathbf{K}(\hat{\mathbf{n}}^{\rm inc})\mathbf{I}^{\rm inc}, \qquad (19b)\end{aligned}$$

where $\boldsymbol{O}(r^{-2})$ is a 4×4 matrix with elements vanishing at infinity as r^{-2}. The third part is described by minus the product of the extinction matrix $\mathbf{K}$ and the Stokes column vector of the incident wave. The elements of the extinction matrix have the dimension of area and are linear combinations of the elements of the forward-scattering amplitude matrix $\mathbf{S}(\hat{\mathbf{n}}^{\rm inc},\hat{\mathbf{n}}^{\rm inc})$.

The situation depicted in Fig. 5 is, in many respects, the embodiment of the concept of light scattering. Indeed, it demonstrates that in the absence of the object, detector 2 would measure no signal, while the signal measured by detector 1 would be proportional to the Stokes column vector of the incident light. In the presence of the object, the readings of both detectors change. The

reading of detector 2 is now proportional to the Stokes column vector of the scattered field, while the polarization signal measured by detector 1 is modified in two ways. First, the total measured intensity is attenuated as a combined result of the scattering of electromagnetic energy by the object in all directions and, possibly, the transformation of electromagnetic energy into other forms of energy (such as heat) inside the object. Second, the modification rates for the four Stokes components of the measured signal can be different. This effect is typical of objects lacking perfect spherical symmetry and is called dichroism. Thus, to describe far-field scattering means, in effect, to quantify the difference between the readings of detectors 1 and 2 in the presence of the object and in the absence of the object. This quantification can be fully achieved in terms of the phase and extinction matrices which depend on object characteristics such as size, shape, refractive index, and orientation and can be readily computed provided that the amplitude scattering matrix is known.

The near field is not, in general, a transverse electromagnetic wave. Therefore, to characterize the response of the "near-field" detectors shown in Fig. 4, one must define quantities other than the Stokes parameters and the extinction and phase matrices. Still the actual observables must be defined in such a way that they can be measured by an optical device ultimately recording the flux of electromagnetic energy. We will see in later sections how this is done in the framework of the theories of RT and CB.

7. FOLDY–LAX EQUATIONS

As we have already mentioned, many theoretical techniques based on directly solving the differential Maxwell equations or their integral counterparts are applicable to an arbitrary fixed finite object, be it a single physical body or a cluster consisting of several distinct components, either touching or spatially separated. These techniques are based on treating the object as a single scatterer and yield the total scattered field. However, if the object is a multi-particle group then it is often convenient to represent the total scattered field as a vector superposition of partial fields scattered by the individual particles. This means that the total electric field at a point **r** is written as follows:

$$\mathbf{E}(\mathbf{r}) = \mathbf{E}^{\rm inc}(\mathbf{r}) + \sum_{i=1}^{N} \mathbf{E}_i^{\rm sca}(\mathbf{r}), \qquad \mathbf{r} \in \Re^3, \tag{20}$$

where N is the number of particles in the group and $\mathbf{E}_i^{\rm sca}(\mathbf{r})$ is the ith partial scattered electric field.

The partial scattered fields can be found by solving vector so-called Foldy–Lax equations (FLEs) which follow directly from the VIE and are exact [34, 43]. Specifically,

$$\mathbf{E}_i^{\rm sca}(\mathbf{r}) = \int_{V_i} d\mathbf{r}' \vec{G}(\mathbf{r}, \mathbf{r}') \cdot \int_{V_i} d\mathbf{r}'' \vec{T}_i(\mathbf{r}', \mathbf{r}'') \cdot \mathbf{E}_i(\mathbf{r}''), \tag{21}$$

where V_i is the volume occupied by the ith particle, $\mathbf{E}_i(\mathbf{r}'')$ is the electric field "exciting" particle i, and the N dyadics $\vec{T}_i$ can be found by solving individually the following Lippmann–Schwinger equation:

$$\vec{T}_i(\mathbf{r}, \mathbf{r}') = k_1^2[m_i^2(\mathbf{r}) - 1]\delta(\mathbf{r} - \mathbf{r}')\vec{I} + k_1^2[m_i^2(\mathbf{r}) - 1]\int_{V_i} d\mathbf{r}'' \vec{G}(\mathbf{r}, \mathbf{r}'') \cdot \vec{T}_i(\mathbf{r}'', \mathbf{r}'), \qquad \mathbf{r}, \mathbf{r}' \in V_i. \tag{22}$$

Comparison with Eq. (6) shows that $\vec{T}_i$ for each i is in fact the dyadic transition operator of particle i with respect to the laboratory coordinate system computed in the absence of all the other particles. Thus, the N dyadic transition operators are totally independent of each other. However, the exciting fields are interdependent and must be found by solving the following system of N linear integral equations:

$$\mathbf{E}_i(\mathbf{r}) = \mathbf{E}^{\rm inc}(\mathbf{r}) + \sum_{j(\neq i)=1}^{N} \int_{V_j} d\mathbf{r}' \ddot{G}(\mathbf{r}, \mathbf{r}') \cdot \int_{V_j} d\mathbf{r}'' \ddot{T}_j(\mathbf{r}', \mathbf{r}'') \cdot \mathbf{E}_j(\mathbf{r}''), \quad \mathbf{r} \in V_i, \quad i = 1, ..., N. \quad (23)$$

In general, the FLEs (20)–(23) are equivalent to Eqs. (5)–(6). However, the fact that $\ddot{T}_i$ for each i is an individual property of the ith particle computed as if this particle were alone allows one to introduce the concept of multiple scattering. This will be the subject of the following section.

One specific, numerically exact approach to solve the FLEs is the so-called superposition T-matrix method which involves the expansion of the various electric fields in vector spherical wave functions centered either at the common origin of the entire scattering object or at the individual particle origins [38, 44, 46, 47]. This technique is especially efficient in application to groups of spherically symmetric particles and will be used in Section 11 to illustrate the scattering effects that can and cannot be described by the theories of RT and CB.

8. WHAT IS MULTIPLE SCATTERING?

Let us rewrite Eqs. (20) and (23) in the following compact operator form:

$$E = E^{\rm inc} + \sum_{i=1}^{N} \hat{G}\hat{T}_i E_i, \quad (24)$$

$$E_i = E^{\rm inc} + \sum_{j(\neq i)=1}^{N} \hat{G}\hat{T}_j E_j, \quad (25)$$

where

$$\hat{G}\hat{T}_j E_j = \int_{V_j} d\mathbf{r}' \ddot{G}(\mathbf{r}, \mathbf{r}') \cdot \int_{V_j} d\mathbf{r}'' \ddot{T}_j(\mathbf{r}', \mathbf{r}'') \cdot \mathbf{E}_j(\mathbf{r}''). \quad (26)$$

Iterating Eq. (26) yields

$$E_i = E^{\rm inc} + \sum_{j(\neq i)=1}^{N} \hat{G}\hat{T}_j E^{\rm inc} + \sum_{\substack{j(\neq i)=1 \\ l(\neq j)=1}}^{N} \hat{G}\hat{T}_j \hat{G}\hat{T}_l E^{\rm inc} + \sum_{\substack{j(\neq i)=1 \\ l(\neq j)=1 \\ m(\neq l)=1}}^{N} \hat{G}\hat{T}_j \hat{G}\hat{T}_l \hat{G}\hat{T}_m E^{\rm inc} + \cdots, \quad (27)$$

whereas substituting Eq. (27) in Eq. (24) gives what can be interpreted as an order-of-scattering expansion of the total electric field:

$$E = E^{\rm inc} + E^{\rm sca}, \quad (28a)$$

$$E^{\rm sca} = \sum_{i=1}^{N} \hat{G}\hat{T}_i E^{\rm inc} + \sum_{\substack{i=1 \\ j(\neq i)=1}}^{N} \hat{G}\hat{T}_i \hat{G}\hat{T}_j E^{\rm inc} + \sum_{\substack{i=1 \\ j(\neq i)=1 \\ l(\neq j)=1}}^{N} \hat{G}\hat{T}_i \hat{G}\hat{T}_j \hat{G}\hat{T}_l E^{\rm inc} + \cdots. \quad (28b)$$

Indeed, the dyadic transition operators are independent of each other, and each of them can be interpreted as a unique and complete electromagnetic identifier of the corresponding particle. Therefore, $\hat{G}\hat{T}_i E^{\rm inc}$ can be interpreted as the partial scattered filed at the observation point generated by particle i in response to the excitation by the incident field only, $\hat{G}\hat{T}_i \hat{G}\hat{T}_j E^{\rm inc}$ is the partial field generated by the same particle in response to the excitation caused by particle j in response to the excitation by the incident field, etc. Thus, the first term on the right-hand side of Eq. (28b) can be interpreted as the sum of all single-scattering contributions, the second term is the sum of all double-scattering contributions, etc. The first term on the right-hand side of Eq. 28(a) represents the unscattered (i.e., incident) field. This order-of-scattering interpretation of Eqs. (28a) and (28b) is visualized in Fig. 6.

We will see very soon that Eqs. (28a) and (28b) constitute a very fruitful way of re-writing the

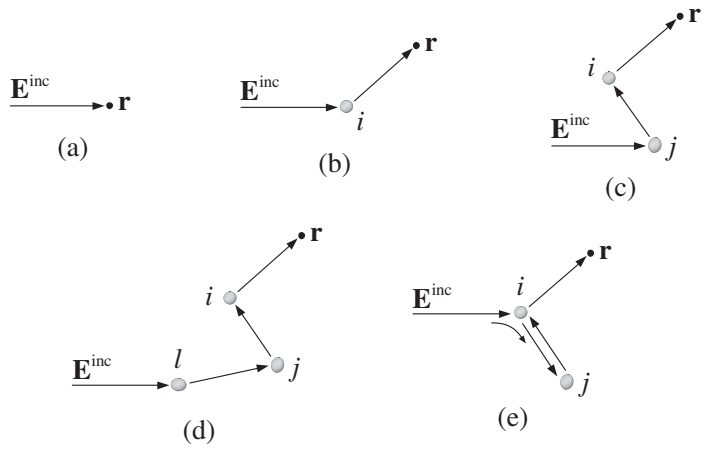

Figure 6. (a) Unscattered (incident) field; (b) single scattering; (c) double scattering; (d), (e) triple scattering.

original FLEs and that the use of the "multiple scattering" terminology is a convenient and compact way of illustrating their numerous consequences [48]. It is important to recognize, however, that beyond being an interpretation and visualization tool, the concept of multiple scattering does not represent a physical process per se. For example, the third term on the right-hand side of Eq. (28b) cannot be interpreted by saying that a light ray (or a localized blob of energy) approaches particle l, gets scattered by particle l towards particle j, approaches particle j, gets scattered by particle j towards particle i, approaches particle i, gets scattered by particle i towards the observation point, and finally arrives at the observation point. Indeed, it follows from Eq. (23) that all mutual particle–particle excitations occur simultaneously and are not temporally discrete and ordered events. The purely mathematical character of the multiple-scattering interpretation of Eq. (28b) becomes especially apparent upon realizing that this equation is quite general and can be applied not only to a multi-particle group but also to a single body wherein the latter is subdivided arbitrarily into N non-overlapping adjacent geometrical regions V_i.

It is convenient to represent the order-of-scattering expansion (28) of the electric field using the diagram method. In Fig. 7, the arrows represent the incident field, the symbol —● denotes the "multiplication" of a field by a $\hat{G}\hat{T}$ dyadic according to Eq. (26), and the dashed curve indicates that two scattering "events" involve the same particle.

9. FAR-FIELD FOLDY–LAX EQUATIONS

We have seen in Section 5 that as a direct consequence of Eqs. (5) and (7), the behavior of the scattered field becomes much simpler in the far-field zone of the scattering object. Since the structure of Eqs. (21) and (23) is analogous to that of Eq. (5), one can expect a similar simplification

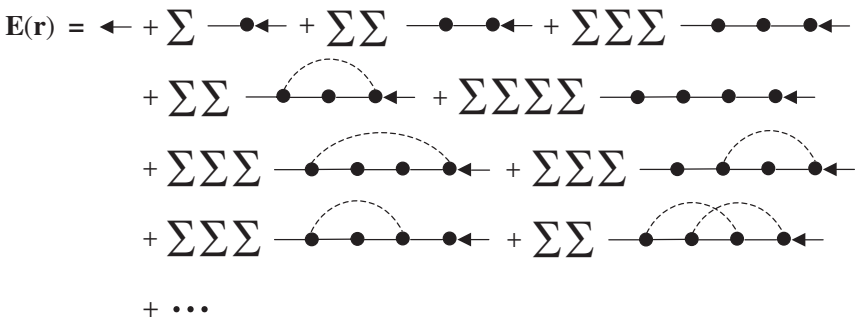

Figure 7. Diagrammatic representation of Eq. (28).

of the FLEs upon making the following two assumptions:

- The N particles forming the group are separated widely enough that each of them is located in the far-field zones of all the other particles.
- The observation point is located in the far-field zone of any particle forming the group.

Indeed, the contribution of the jth particle to the field exciting the ith particle in Eq. (23) can now be represented as a simple outgoing spherical wavelet centered at the origin of particle j. By the time this wavelet reaches particle i its radius of curvature becomes much larger than the size of particle i so that the wavelet can be considered as *locally* plane. The scattering of this wavelet by particle i can then be described in terms of the corresponding scattering dyadic $\vec{A}_i$, Eq. (8). As a result, the system of integral FLEs turns into a system of algebraic equations [38].

Specifically, assuming that the incident field is a plane electromagnetic wave propagating in the direction $\hat{\mathbf{n}}^{\rm inc}$, we have for the total field at a point $\mathbf{r}$ located in the far-field zone of all the particles:

$$\mathbf{E}(\mathbf{r}) = \mathbf{E}^{\rm inc}(\mathbf{r}) + \sum_{i=1}^{N} G(r_i)\vec{A}_i(\hat{\mathbf{r}}_i, \hat{\mathbf{n}}^{\rm inc})\cdot\mathbf{E}^{\rm inc}(\mathbf{R}_i) + \sum_{i=1}^{N} G(r_i)\sum_{j(\neq i)=1}^{N}\vec{A}_i(\hat{\mathbf{r}}_i, \hat{\mathbf{R}}_{ij})\cdot\mathbf{E}_{ij}, \tag{29}$$

where $G(r) = \exp(\mathrm{i}k_1 r)/r$, r_i is the distance between the origin of particle i and the observation point, $\hat{\mathbf{r}}_i$ the unit vector directed from the origin of particle i towards the observation point, $\mathbf{R}_i$ is the position vector of the ith particle origin, and $\hat{\mathbf{R}}_{ij}$ is the unit vector directed from the origin of particle j towards the origin of particle i. Equation (29) shows that the total field at any point located sufficiently far from any particle in the group is the superposition of the incident plane wave and N spherical waves generated by the N particles. The amplitudes of the particle–particle excitations $\mathbf{E}_{ij}$ are found from the following system of $N(N-1)$ linear algebraic equations:

$$\begin{gathered}\mathbf{E}_{ij} = G(R_{ij})\vec{A}_j(\hat{\mathbf{R}}_{ij}, \hat{\mathbf{n}}^{\rm inc})\cdot\mathbf{E}^{\rm inc}(\mathbf{R}_j) + G(R_{ij})\sum_{l(\neq j)=1}^{N}\vec{A}_j(\hat{\mathbf{R}}_{ij}, \hat{\mathbf{R}}_{jl})\cdot\mathbf{E}_{jl},\\ i, j = 1, ..., N, \qquad j \neq i,\end{gathered} \tag{30}$$

where R_{ij} is the distance between the origins of particles j and i.

This system is much simpler than the original system of FLEs and can, in principle, be solved with a computer provided that N is not too large. The expression for the order-of-scattering expansion of the total field also becomes much simpler:

$$\begin{aligned}\mathbf{E} = \mathbf{E}^{\rm inc} &+ \sum_{i=1}^{N}\vec{B}_{ri0}\cdot\mathbf{E}_i^{\rm inc} + \sum_{i=1}^{N}\sum_{j(\neq i)=1i}^{N}\vec{B}_{rij}\cdot\vec{B}_{ij0}\cdot\mathbf{E}_j^{\rm inc} + \sum_{i=1}^{N}\sum_{j(\neq i)=1}^{N}\sum_{l(\neq j)=1}^{N}\vec{B}_{rij}\cdot\vec{B}_{ijl}\cdot\vec{B}_{jl0}\cdot\mathbf{E}_l^{\rm inc}\\ &+ \sum_{i=1}^{N}\sum_{j(\neq i)=1}^{N}\sum_{l(\neq j)=1}^{N}\sum_{m(\neq l)=1}^{N}\vec{B}_{rij}\cdot\vec{B}_{ijl}\cdot\vec{B}_{jlm}\cdot\vec{B}_{lm0}\cdot\mathbf{E}_m^{\rm inc} + \cdots,\end{aligned} \tag{31}$$

where

$$\mathbf{E} = \mathbf{E}(\mathbf{r}), \qquad \mathbf{E}^{\rm inc} = \mathbf{E}^{\rm inc}(\mathbf{r}), \qquad \mathbf{E}_i^{\rm inc} = \mathbf{E}^{\rm inc}(\mathbf{R}_i), \tag{32}$$

$$\vec{B}_{ri0} = G(r_i)\vec{A}_i(\hat{\mathbf{r}}_i, \hat{\mathbf{n}}^{\rm inc}), \tag{33}$$

$$\vec{B}_{rij} = G(r_i)\vec{A}_i(\hat{\mathbf{r}}_i, \hat{\mathbf{R}}_{ij}), \tag{34}$$

$$\vec{B}_{ij0} = G(R_{ij})\vec{A}_j(\hat{\mathbf{R}}_{ij}, \hat{\mathbf{n}}^{\rm inc}), \tag{35}$$

$$\vec{B}_{ijl} = G(R_{ij})\vec{A}_j(\hat{\mathbf{R}}_{ij}, \hat{\mathbf{R}}_{jl}). \tag{36}$$

The remarkable feature of the above formulas is that now the role of the unique

electromagnetic identifier of each particle is assumed by the corresponding scattering dyadic, that is, the same quantity that would completely describe far-field scattering by this particle if it were alone rather than a member of the group. Although the dyadic transition operator is the most general electromagnetic property of a particle, the scattering dyadic or, equivalently, the amplitude scattering matrix have been used so frequently to describe far-field scattering by a particle that they have become almost synonymic with the words "single scattering". This appears to add some notoriety to the order-of-scattering interpretation of Eq. (31). One should not forget, however, that Eq. (31) is just an approximate version of Eq. (28) and does not make multiple scattering a real physical process.

The diagrammatic formula shown in Fig. 7 can also represent Eq. (31) provided that the symbol —● is now interpreted as the multiplication of a field by a $\vec{B}$ dyadic.

10. ERGODICITY

Most of our discussion of electromagnetic scattering in the previous sections has been based on the assumption that the configuration of the scattering object with respect to the laboratory reference frame is fixed. However, quite often one has to deal with an object in the form of a multi-particle group in which the particles are randomly rotating and moving relative to each other. The particles may even change there sizes and shapes owing to evaporation, sublimation, condensation, or melting. Important examples of such "stochastic" scattering objects are clouds consisting of water droplets and/or ice crystals, plumes of aerosol particles, and various particle suspensions. The physical and chemical processes controlling the temporal evolution of such objects can be extremely complex and convoluted.

Although a random group can be described at any given moment in terms of a specific fixed particle configuration, any measurement takes a finite amount of time during which the group goes through an infinite sequence of evolving discrete configurations. Sometimes the result of the measurement can be modeled numerically by solving the Maxwell equations for many time-sequential discrete configurations and then taking the average. A far more practical approach in most cases is based on the assumption of ergodicity. Specifically, all further discussion will be based on the following two fundamental premises:

- The scattering object can be adequately characterized at any moment in time by a finite set of physical parameters.
- The scattering object is sufficiently variable in time and the time interval necessary to take a measurement is sufficiently long that averaging the scattering signal over this interval is essentially equivalent to averaging the signal over an appropriate analytical probability distribution of the physical parameters characterizing the scattering object.

In other words, we will assume that averaging over time for one specific realization of a random scattering process is equivalent to ensemble averaging.

To better understand the meaning of ergodicity, let us consider the measurement of a scattering characteristic A of a cloud of spherical water droplets. This characteristic depends on time implicitly by being a function of time-dependent physical parameters of the cloud such as the coordinates and radii of all the constituent particles. The full set of particle positions and radii will be denoted collectively by ψ and determines the state of the entire cloud at a moment in time. In order to interpret the measurement of $A[\psi(t)]$ accumulated over a period of time extending from $t = t_0$ to $t = t_0 + T$, one needs a way of predicting theoretically the average value

$$\overline{A} = \frac{1}{T}\int_{t_0}^{t_0+T} \mathrm{d}t\, A[\psi(t)]. \tag{37}$$

As we have already mentioned, the temporal evolution of the cloud of water droplets is

described by an intricate system of equations representing the various physical and chemical processes in action. To incorporate the solution of this system of equations for each moment of time into the theoretical averaging procedure (37) can be a formidable task and is never done. Instead, averaging over time is replaced by ensemble averaging based on the following rationale.

Although the coordinates and sizes of water droplets in the cloud change with time in a specific way, the range of instantaneous states of the cloud captured by the detector during the measurement becomes representative of that captured over an infinite period of time provided that T is sufficiently large. We thus have

$$\overline{A} \approx \lim_{\tau \to \infty} \frac{1}{\tau} \int_{t_0}^{t_0+\tau} \mathrm{d}t\, A[\psi(t)] = \langle A \rangle_t. \tag{38}$$

Notice now that the infinite integral in Eq. (38) can be expected to "sample" every physically realizable state ψ of the cloud. Furthermore, this sampling is statistically representative in that the number of times each state is sampled is large and tends to infinity in the limit $\tau \to \infty$. Most importantly, the cumulative contribution of a cloud state ψ to $\langle A \rangle_t$ is independent of the specific moments in time when this state actually occurred in the process of the temporal evolution of the cloud. Rather, it depends on how many times this state was sampled. Therefore, this cumulative contribution can be thought of as being proportional to the probability of occurrence of the state ψ at *any* moment of time. This means that instead of specifying the state of the cloud at each moment t and integrating over all t, one can introduce an appropriate time-independent probability density function $p(\psi)$ and integrate over the entire physically realizable range of cloud states:

$$\langle A \rangle_t \approx \int \mathrm{d}\psi\, p(\psi) A(\psi) = \langle A \rangle_\psi, \tag{39}$$

where

$$\int \mathrm{d}\psi\, p(\psi) = 1. \tag{40}$$

Equation (39) is the formal mathematical expression of the principle of ergodicity introduced above. Physical processes such as Brownian motion and turbulence often help to establish a significant degree of randomness of particle positions and orientations, which seems to explain why many theoretical predictions based on the ergodic hypothesis have agreed very well with experimental data [50]. The practical meaning of ergodicity in the framework of the theories of RT and CB will be discussed in Section 12.

11. MULTIPLE SCATTERING BY RANDOM PARTICULATE MEDIA: EXACT RESULTS

The far-field FLEs provide the foundation necessary to develop the microphysical theories of RT and CB. However, before proceeding with the outline of these inherently approximate theories, in this section we will use *numerically exact* results in order to develop an understanding of what further assumptions and approximations will be necessary and what specific scattering effects these theories may or may not be expected to encompass. To this end, we will analyze T-matrix results computed for a macroscopic volume filled with randomly distributed wavelength-sized particles [49]. We have already mentioned that, for practical reasons, the superposition T-matrix method cannot be used yet to handle random media consisting of very large numbers of particles such as clouds, colloids, and powder surfaces. However, it does provide the potential to model rather complex particulate systems and thereby simulate the effect of randomness of particle positions as well as the onset and evolution of various "multiple-scattering" effects with increasing number of particles in a statistically homogeneous volume of discrete random medium.

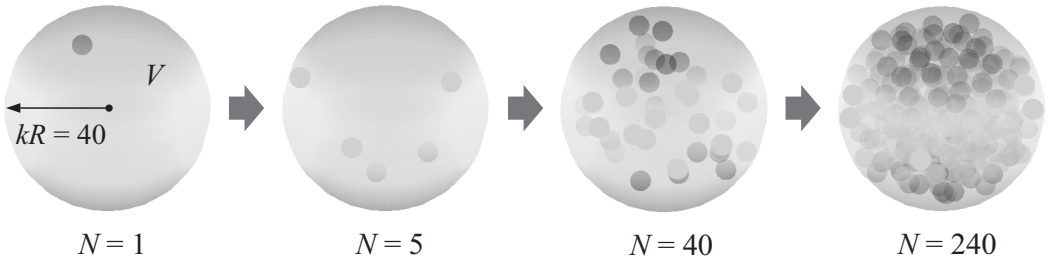

Figure 8. N particles are distributed randomly throughout a spherical volume V of the host medium.

11.1. Static and dynamic light scattering

We assume that a number N of identical spherical particles are distributed randomly throughout a spherical volume V with a radius R much greater than the particle radius a, as shown in Fig. 8. The size parameter of the particles is fixed at $k_1a = 4$, whereas the size parameter of the spherical volume is fixed at $k_1R = 40$. The refractive index of the particles relative that of the surrounding medium is 1.32.

As we have explained above, in order to simulate measurements of light scattering by a rapidly changing object one needs to solve the Maxwell equations repeatedly for a representative set of distinct object configurations. After the set of solutions of the Maxwell equations has been obtained, one has a choice of (i) analyzing the statistical information content of differences in the individual solutions or (ii) applying an averaging procedure and thereby isolating the static component of the scattering pattern. These two approaches are known as *dynamic* and *static* light scattering [34, 50, 51].

To model numerically dynamic light scattering by the statistically homogeneous volume of random particulate medium, one needs a procedure that assigns coordinates to particles forming a specific realization of the random N-particle group filling the volume. In our computations, we have used two approaches. The first one uses a random-number generator to assign sequentially 3D coordinates to each of the N particles based on a trial-and-error procedure ensuring that the particles do not overlap. The second one is a slightly modified version of the procedure described in [52].

To simulate static light scattering, one needs an efficient way of averaging the computed scattering signal over very many configurations of the N-particle group. A brute-force solution would be to use a random coordinate generator repeatedly to create a large number of different N-particle configurations and then average numerically the corresponding T-matrix results. The more effective approach used here is to create only one random N-particle configuration and then average over all possible orientations of this configuration with respect to the laboratory coordinate system. This procedure yields an infinite continuous set of random realizations of the N-particle group and takes full advantage of the highly efficient orientation averaging procedure afforded by the superposition T-matrix method [38, 53].

11.2. Fixed configurations of randomly positioned particles: speckle

Let us assume that the large spherical volume V is illuminated by a plane electromagnetic wave. The incidence direction coincides with the positive direction of the z-axis of the laboratory reference frame and the meridional plane of the incidence direction coincides with the xz half-plane with $x \geq 0$ (cf. Fig. 3(a)). The angular distribution and polarization state of the scattered light in the far-field zone of the entire scattering volume is described by the Stokes phase matrix $\mathbf{Z}$, Eq. (18).

Let us first assume that the incident light is circularly polarized in the counter-clockwise sense when viewed in the direction of propagation, which implies that $V^{\rm inc} = I^{\rm inc}$ and $Q^{\rm inc} = U^{\rm inc} = 0$. Panels (a) and (b) of Fig. 9 show the far-field angular distributions of the intensity $I^{\rm sca}$ scattered in

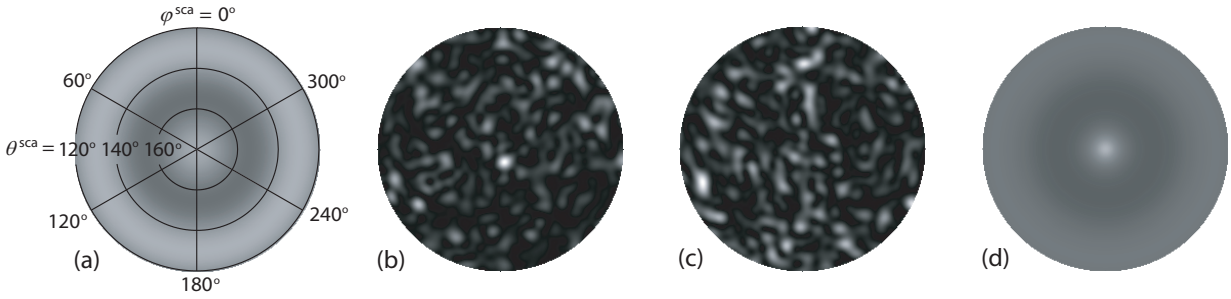

Figure 9. Angular distribution of scattered intensity in the far-field zone of the spherical volume V filled with N particles. (a) $N = 1$, fixed orientation. (b) and (c) $N = 80$, fixed orientation. (d) $N = 80$, random orientation. The gray scale is individually adjusted in order to maximally reveal the details of each scattering pattern. Panel (a) also shows the angular coordinates used for all panels.

the backward hemisphere by the large spherical volume filled with $N = 1$ and 80 particles having the same refractive index $m = 1.32$. The individual particle positions were chosen randomly using a random coordinate generator, but otherwise they are fixed. The scattering pattern for $N = 1$ is rather smooth and perfectly azimuthally symmetric, as it should be for a single wavelength-sized spherical particle. However, panel (b) demonstrates a typical speckle pattern.

The origin of the speckle can be explained as follows. Equations (28b) and (7) suggest that at a distant observation point, the partial field due to any particle sequence contributing to the right-hand side of Eq. (28b) becomes an outgoing spherical wavelet centered at the last particle of the sequence. This occurs irrespective of whether the particles are densely packed or sparsely distributed. The Stokes parameters of the scattered light can be directly expressed in terms of the elements of the scattering coherency dyad $\mathbf{E}^{sca} \otimes (\mathbf{E}^{sca})^*$. The dyadic product of the right-hand side of Eq. (28b) and its complex-conjugate counterpart is the sum of an infinite number of terms, each describing the result of interference of two wavelets scattered along sertain particle sequences.

Two such particle sequences are shown in Fig. 10. If the interference of the corresponding wavelets is constructive (destructive) then it serves to increase (decrease) the total intensity scattered in the direction $\hat{\mathbf{n}}^{sca}$. The total intensity is the sum of the interference results contributed by all possible pairs of scattering sequences. The typical angular width of each interference maximum or minimum is proportional to $1/k_1 R$, whereas the number of these maxima and minima grows swiftly with increasing N. These two factors explain the spotty appearance of the scattering pattern in panel 9(b).

Of course, the speckle pattern depends not only on the number of particles N but also on the specific way they are arranged with respect to the laboratory coordinate system. This is illustrated by panels 9(b) and 9(c) computed for two different random 80-particle configurations.

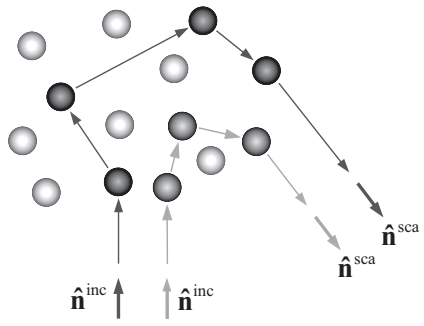

Figure 10. Interference origin of speckle.

11.3. Static scattering

Figures 9(b) and 9(c) illustrate the range of variability of the speckle pattern that can be expected upon even minute changes in a random multi-particle configuration. Obviously, neither the speckle pattern nor its variability are reproduced by the classical theories of RT and CB, which indicates that *neither theory describes the instantaneous state of electromagnetic radiation* in a discrete random medium. Instead, both theories fall in the realm of static scattering and describe the result of averaging the relevant optical observables over a significant period of time or, equivalently, over a significant range of random particle positions.

To illustrate this fundamental point, Fig. 9(d) shows the result of averaging the speckle pattern over the uniform orientation distribution of the 80-particle configuration used to compute Fig. 9(b). One can see that with the exception of a notable backscattering peak, the speckle structure is essentially gone. This is not surprising. Indeed, each speckle element is the result of constructive or destructive interference of two wavelets scattered along specific particle sequences such as those shown in Fig. 10. The phase difference between the wavelets changes randomly as the particles move, so that the average result of the interference is zero. However, there are certain pairs of wavelets that interfere constructively irrespective of particle positions and thereby are responsible for the residual scattering pattern. We will demonstrate below that the backscattering intensity peak seen in Fig. 9(d) as well as the smooth intensity background are in fact caused by special classes of such wavelet pairs.

In what follows, we employ the concept of multiple scattering to interpret various effects of increasing the number of particles filling the scattering volume on the static scattering patterns obtained by averaging over all orientations of a random N-particle configuration with respect to the laboratory reference frame. We make a simplifying assumption that $\varphi^{\rm sca} = 0$ and define the scattering direction in terms of the scattering angle $\Theta = \theta^{\rm sca}$. Then the scattering process can be conveniently described in terms of the so-called normalized Stokes scattering matrix [34, 38] which is a particular case of the phase matrix and is given by

$$\begin{bmatrix} a_1(\Theta) & b_1(\Theta) & 0 & 0 \\ b_1(\Theta) & a_2(\Theta) & 0 & 0 \\ 0 & 0 & a_3(\Theta) & b_2(\Theta) \\ 0 & 0 & -b_2(\Theta) & a_4(\Theta) \end{bmatrix}. \tag{41}$$

The specific block-diagonal structure of this matrix is confirmed by the numerically exact T-matrix results and is largely caused by averaging over the uniform orientation distribution of a multi-particle group coupled with sufficient randomness of particle positions throughout the scattering volume. All scattering matrix elements denoted in Eq. (41) by a zero have been found to be at least an order of magnitude smaller than the smallest non-zero element (in the absolute-value sense). The (1,1) element, called the phase function, satisfies the following normalization condition:

$$\frac{1}{2}\int_0^{\pi} {\rm d}\Theta \sin\Theta \, a_1(\Theta) \; = \; 1. \tag{42}$$

The phase function describes the angular distribution of the scattered intensity provided that the incident light is unpolarized.

The upper left-hand panel of Fig. 11 vividly demonstrates several fundamental consequences of increasing the number of particles in the scattering volume. First, the constructive interference of light singly scattered by the component particles in the exact forward direction causes a strong forward-scattering enhancement [34]. This feature can be called forward-scattering localization of light. It is further detailed in the upper right-hand panel of Fig. 11 and explained in Fig. 12. Indeed, the exact forward-scattering direction is unique in that the phase of the wavelets singly forward-scattered by all the particles in the volume is exactly the same irrespective of the specific particle positions, Fig. 12(a). In the absence of multiple scattering, the constructive interference of these

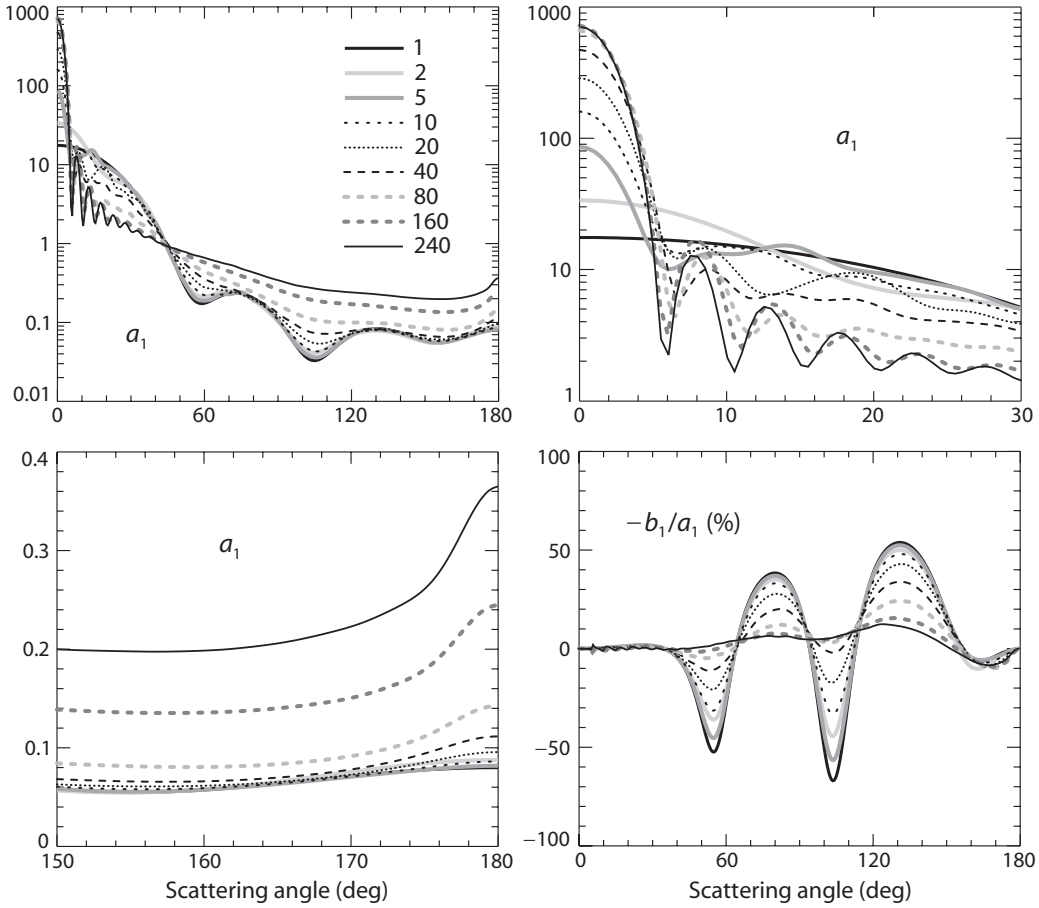

Figure 11. Phase function and the ratio $-b_1/a_1$ computed for the volume V of discrete random medium filled with a varying number of particles.

wavelets would lead to an increase of the forward-scattering phase function $a_1(0°)$ by a factor of N. This increase does occur for $N = 2$ and 5, but then is slows down, and by the time N reaches the value 160 the $a_1(0°)$ value saturates. This behavior can be interpreted in terms of a multiple-scattering effect whereby particle 3 (see the right-hand particle sequence in Fig. 12(b)) "shades" particle 2 by attenuating the incident field exciting particle 2. In fact, it is this multiple-scattering effect that leads to the exponential extinction law in the framework of the RT theory.

Second, the phase functions at scattering angles $\Theta > 170°$ start to develop a backscattering enhancement which becomes quite pronounced for $N \geq 160$ (see the bottom left-hand diagram of Fig. 11). This feature has an angular width also indicative of an interference origin and is, in fact, a typical manifestation of the so-called coherent backscattering (CB) effect. The standard explanation of CB is illustrated in Fig. 13(a) and is as follows. The conjugate wavelets scattered along the same string of n particles but in opposite directions interfere in the far-field zone, the interference being constructive or destructive depending on the respective phase difference,

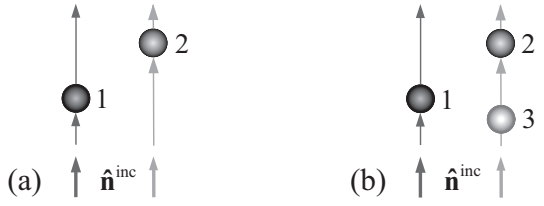

Figure 12. Forward-scattering interference.

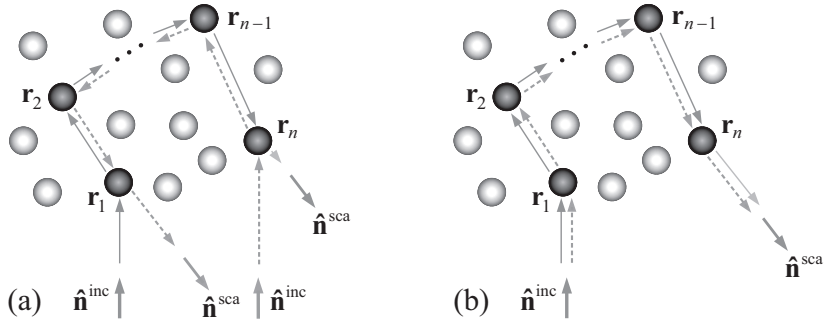

Figure 13. Interference origin of (a) CB and (b) diffuse background.

$$\Delta = k_1(\mathbf{r}_n - \mathbf{r}_1)\cdot(\hat{\mathbf{n}}^{\mathrm{inc}} + \hat{\mathbf{n}}^{\mathrm{sca}}). \tag{43}$$

If the observation direction $\hat{\mathbf{n}}^{\mathrm{sca}}$ is far from the exact backscattering direction given by $-\hat{\mathbf{n}}^{\mathrm{inc}}$ then the average effect of interference of the conjugate wavelets scattered along various strings of particles is zero, owing to randomness of particle positions. However, at exactly the backscattering direction, $\hat{\mathbf{n}}^{\mathrm{sca}} = -\hat{\mathbf{n}}^{\mathrm{inc}}$, the phase difference between the conjugate paths involving *any* string of particles is identically equal to zero, and the interference is always constructive and causes an intensity peak.

It is important to recognize that the very concept of wave phase applies only to transverse waves such as plane and spherical waves. Therefore, the above explanation of CB is implicitly based on the assumption that each particle in the particle string, Fig. 13(a), is located in the far-field zones of the previous and the following particle. However, the presence of a strong CB peak even in the phase function computed for 240 densely packed particles (cf. the right-most panel of Fig. 8) indicates that the wavelets scattered along strings of widely separated particles still provide a significant contribution to the total scattered signal.

The third consequence of increasing N is that the phase functions at scattering angles $30^\circ \le \Theta \le 170^\circ$ become progressively smooth and featureless, thereby causing the "diffuse" intensity background clearly identifiable in Fig. 9(d). The major contributor to the background intensity is another class of wavelet pairs as illustrated in Fig. 13(b). Now the wavelet scattered along a string of n particles interferes with itself. Since the corresponding phase difference is exactly equal to zero irrespective of particle positions, the self-interference is always constructive. The smoothness of the background intensity can again be interpreted as a typical result of increasing amount of multiple scattering whereby light undergoing many scattering events "forgets" the initial incidence direction $\hat{\mathbf{n}}^{\mathrm{inc}}$ and is more likely to contribute equally to all "exit" directions $\hat{\mathbf{n}}^{\mathrm{sca}}$.

The degree of linear polarization of the scattered light for unpolarized incident light is given by the ratio $-b_1/a_1$. The bottom right-hand panel in Fig. 11 shows that the most obvious effect of increasing N is to smooth out the oscillations in the polarization curve for the single wavelength-sized sphere and, on average, to make polarization more neutral. The standard multiple-scattering explanation of this trait is that the main contribution to the second Stokes parameter, Q^{sca}, comes from the first order of scattering, whereas light scattered many times, Fig. 13(b), becomes largely unpolarized.

The three fundamental classes of wavelet pairs illustrated in Figs. 12 and 13 are the main contributors to the scattering patterns shown in Figs. 9(d) and 11. In the following sections we will see how and to what extent they are incorporated in the theories of RT and CB.

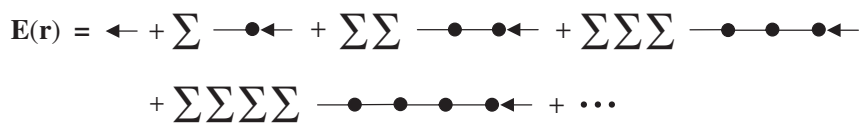

Figure 14. The Twersky approximation.

12. RADIATIVE TRANSFER THEORY

We are now well prepared to proceed with the outline of the RT theory by considering the scattering of a plane electromagnetic wave by a large group of N particles randomly distributed throughout a large 3D volume V. In accordance with the above discussion, the derivation of the RTE involves several fundamental premises and approximations. The first one is to assume that each particle is located in the far-field zones of all the other particles and that the observation point is also located in the far-field zones of all the particles forming the scattering medium. As we have seen, this assumption leads to a dramatic simplification of the FLEs wherein the latter are converted from a system of volume integral equations into a system of linear algebraic equations. However, it also limits the applicability of the final result by requiring that the particles in the scattering medium are not closely spaced, a condition that is nonetheless met in many natural circumstances.

The order-of-scattering form of the far-field FLEs, Eq. (31), allows one to represent the total electric field at a point in space as a sum of contributions arising from light-scattering paths going through all possible particle sequences. The second major assumption, called the Twersky approximation [34, 54], is that all paths going through a particle more than once can be neglected. It is straightforward to demonstrate that doing this is justified provided that the number of particles in the scattering volume, N, is very large. Thus, instead of the diagrammatic equation depicted in Fig. 7 we will work with a simplified version depicted in Fig. 14.

The third major assumption is that of full ergodicity, which allows one to replace averaging over time by averaging over particle positions and states, Section 10. The fourth major assumption is that

- the position and state of each particle are statistically independent of each other and of those of all the other particles, and
- the spatial distribution of the particles throughout the medium is random and statistically uniform.

As one might expect, this assumption leads to a major simplification of all analytical derivations. The practical meaning of ergodicity and uniformity will be discussed at the end of this section.

The next major step is the characterization of the multiply scattered radiation by the coherency dyadic

$$\ddot{C}(\mathbf{r}) = \langle \mathbf{E}(\mathbf{r},t) \otimes \mathbf{E}^{*}(\mathbf{r},t) \rangle_{t} \approx \langle \mathbf{E}(\mathbf{r}) \otimes \mathbf{E}^{*}(\mathbf{r}) \rangle_{\mathbf{R},\xi}, \tag{44}$$

where the subscripts $\mathbf{R}$ and ξ denote averaging over all particle coordinates and states, respectively. The state of a particle can collectively indicate its size, refractive index, shape, orientations, etc. The coherency dyadic is appropriately defined as a non-vanishing quantity, Section 6. Because of the averaging over particle coordinates, $\ddot{C}(\mathbf{r})$ is a continuous function of the position vector. Furthermore, as we will see later, the coherency dyadic allows the definition of derivative quantities which are observable directly.

The Twersky expansion of the coherency dyadic is depicted diagrammatically in Fig. 15. To classify the different terms entering the expanded expression inside the angular brackets on the right-hand side of this equation, we will use the notation illustrated in Fig. 16(a). In this particular case, the upper and the lower scattering paths go through different particles. However, the two paths can involve one or more common particles, as shown in panels (c) and (d) by using the dashed

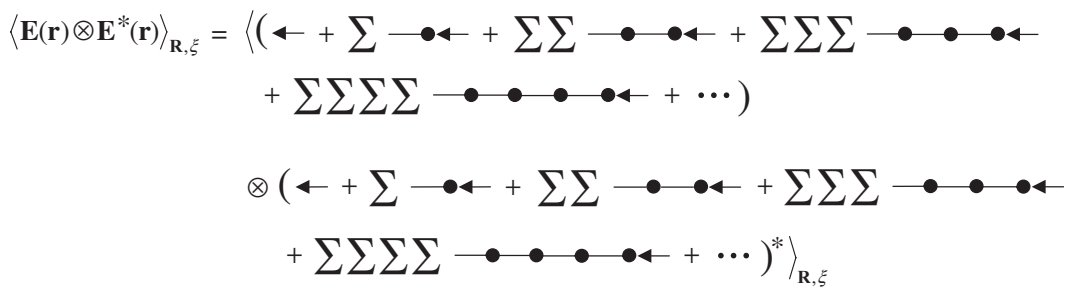

Figure 15. The Twersky expansion of the coherency dyadic.

connectors. Furthermore, if the number of common particles is two or more, they can enter the upper and lower paths in the same order, as in panel (c), or in the reverse order, as in panel (d). Panel (e) shows a mixed diagram in which two common particles appear in the same order and two other common particles appear in the reverse order. The contribution of this diagram to the coherency dyadic is simply

$$[\vec{\vec{B}}_{rij}\cdot\vec{\vec{B}}_{ijk}\cdot\vec{\vec{B}}_{jkl}\cdot\vec{\vec{B}}_{kl0}\cdot\mathbf{E}_l^{\mathrm{inc}}]\otimes[\vec{\vec{B}}_{rik}\cdot\vec{\vec{B}}_{ikj}\cdot\vec{\vec{B}}_{kjl}\cdot\vec{\vec{B}}_{jl0}\cdot\mathbf{E}_l^{\mathrm{inc}}]^*. \tag{45}$$

By the nature of the Twersky approximation, neither the upper path nor the lower path can go through a particle more than once. Therefore, no particle can be the origin of more than one connector.

The next major assumption in the derivation of the RTE is that all diagrams with crossing connectors can be neglected. The rationale for making this assumption can be illustrated by considering the contribution of the term depicted in Fig. 16(e) to the coherency dyadic. Indeed, by substituting Eqs. (33)–(36) in Eq. (45), we see that the resulting expression includes a rapidly oscillating exponential factor

$$\exp[\mathrm{i}k_1(R_{ij}+R_{kl}-R_{ik}-R_{jl})]. \tag{46}$$

This factor causes the contribution of this term to vanish upon averaging over the positions of particles j and k within the volume V provided that all linear dimensions of the volume are much greater than the wavelength of the incident light. However, there is a class of diagrams with crossing connectors which can give a non-vanishing contribution to coherency dyadic. This class will be discussed in Section 13.

Let us now consider the contribution of the diagrams with no crossing connectors like the one

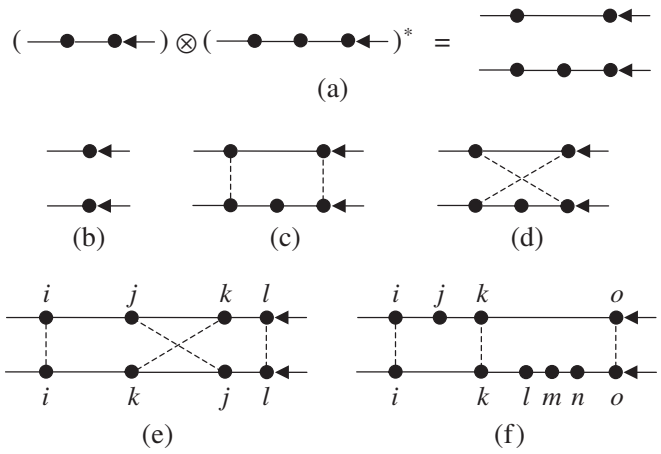

Figure 16. Classification of terms entering the Twersky expansion of the coherency dyadic.

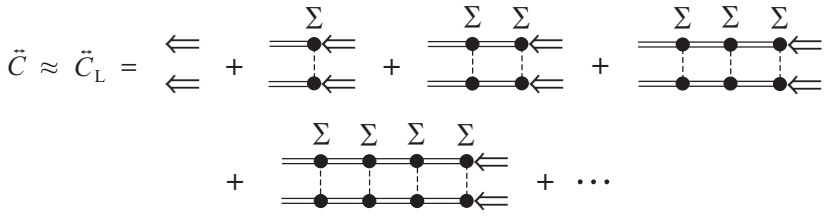

Figure 17. Ladder approximation for the coherency dyadic.

shown in Fig. 16(f). The presence of unconnected particle j in the upper scattering path causes an exponential factor

$$\exp[\mathrm{i}k_1(R_{ij} + R_{jk})] \tag{47}$$

which oscillates rapidly everywhere in V except along the straight line connecting the origins of particles i and k, where this factor is constant. The stationary-phase evaluation of the integral describing the average over all positions of particle j yields a very important result: the only effect particle j has in the context of this specific diagram is to attenuate the field generated by particle k and exciting particle i and to potentially cause dichroism. Similarly, particles l, m, and n have any effect only when they all are positioned along the straight line connecting the origins of particles k and o, and this effect is again to cause attenuation and, possibly, dichroism.

Careful analytical evaluation of the cumulative position- and state-averaged contribution of all diagrams with vertical connectors coupled with the assumption that N is very large leads to the equation depicted diagrammatically in Fig. 17 [34]. The symbol $\Leftarrow$ denotes the incident field attenuated by the unconnected particles on its way to the observation point or to the right-most connected particle, the double lines denote similar attenuation by unconnected particles of a wave propagating from one connected particle to another, and the symbols Σ denote both the summation and over all appropriate particles and the averaging over particle positions and states. Owing to their appearance, the diagrams on the right-hand side of this equation are called ladder diagrams. Therefore, this diagrammatic formula can be called the ladder approximation for the coherency dyadic.

The expanded expression for the ladder coherency dyadic has the form of an angular decomposition in terms of the so-called ladder specific coherency dyadic $\ddot{\Xi}_{\mathrm{L}}(\mathbf{r}, \hat{\mathbf{q}})$:

$$\ddot{C}_{\mathrm{L}}(\mathbf{r}) = \int_{4\pi} \mathrm{d}\hat{\mathbf{q}}\, \ddot{\Xi}_{\mathrm{L}}(\mathbf{r}, \hat{\mathbf{q}}), \tag{48}$$

where the integration is performed over all propagation directions as specified by the unit vector $\hat{\mathbf{q}}$. Furthermore, it is straightforward to show that the specific coherency dyadic satisfies an integral RTE [34].

The ladder specific coherency dyadic can, in turn, be used to define the so-called specific intensity column vector,

$$\widetilde{\mathbf{I}}(\mathbf{r}, \hat{\mathbf{q}}) = \begin{bmatrix} \widetilde{I}(\mathbf{r}, \hat{\mathbf{q}}) \\ \widetilde{Q}(\mathbf{r}, \hat{\mathbf{q}}) \\ \widetilde{U}(\mathbf{r}, \hat{\mathbf{q}}) \\ \widetilde{V}(\mathbf{r}, \hat{\mathbf{q}}) \end{bmatrix}, \tag{49}$$

which also satisfies an integral RTE. The latter can be converted into the following classical integro-differential form:

$$\hat{\mathbf{q}} \cdot \nabla \widetilde{\mathbf{I}}(\mathbf{r}, \hat{\mathbf{q}}) = -n_0 \langle \mathbf{K}(\hat{\mathbf{q}}) \rangle_{\xi} \widetilde{\mathbf{I}}(\mathbf{r}, \hat{\mathbf{q}}) + n_0 \int_{4\pi} \mathrm{d}\hat{\mathbf{q}}' \langle \mathbf{Z}(\hat{\mathbf{q}}, \hat{\mathbf{q}}') \rangle_{\xi} \widetilde{\mathbf{I}}(\mathbf{r}, \hat{\mathbf{q}}'). \tag{50}$$

In this equation, $\langle \mathbf{K}(\hat{\mathbf{q}}) \rangle_\xi$ and $\langle \mathbf{Z}(\hat{\mathbf{q}}, \hat{\mathbf{q}}') \rangle_\xi$ are the extinction and the phase matrix, respectively, averaged over all particle states and $n_0 = N/V$ is the particle number density. The specific intensity column vector can be decomposed into the coherent and diffuse parts,

$$\widetilde{\mathbf{I}}(\mathbf{r}, \hat{\mathbf{q}}) = \delta(\hat{\mathbf{q}} - \mathbf{n}^{\text{inc}}) \mathbf{I}_{\text{c}}(\mathbf{r}) + \widetilde{\mathbf{I}}_{\text{d}}(\mathbf{r}, \hat{\mathbf{q}}), \tag{51}$$

each satisfying its own RTE:

$$\mathbf{n}^{\text{inc}} \cdot \nabla \mathbf{I}_{\text{c}}(\mathbf{r}) = -n_0 \langle \mathbf{K}(\mathbf{n}^{\text{inc}}) \rangle_\xi \mathbf{I}_{\text{c}}(\mathbf{r}), \tag{52}$$

$$\hat{\mathbf{q}} \cdot \nabla \widetilde{\mathbf{I}}_{\text{d}}(\mathbf{r}, \hat{\mathbf{q}}) = -n_0 \langle \mathbf{K}(\hat{\mathbf{q}}) \rangle_\xi \widetilde{\mathbf{I}}_{\text{d}}(\mathbf{r}, \hat{\mathbf{q}}) + n_0 \int_{4\pi} \mathrm{d}\hat{\mathbf{q}}' \langle \mathbf{Z}(\hat{\mathbf{q}}, \hat{\mathbf{q}}') \rangle_\xi \widetilde{\mathbf{I}}_{\text{d}}(\mathbf{r}, \hat{\mathbf{q}}') + n_0 \langle \mathbf{Z}(\hat{\mathbf{q}}, \mathbf{n}^{\text{inc}}) \rangle_\xi \mathbf{I}_{\text{c}}(\mathbf{r}). \tag{53}$$

$\mathbf{I}_{\text{c}}$ reduces to the Stokes column vector of the incident wave at the illuminated boundary of the medium, but is subject to exponential attenuation and, possibly, the effect of dichroism inside the medium.

The RTE becomes considerably simpler in the case of plane-parallel, macroscopically isotropic and mirror-symmetric scattering media [17, 34]:

$$u \frac{\mathrm{d}\widetilde{\mathbf{I}}(\tau, \hat{\mathbf{q}})}{\mathrm{d}\tau} = -\widetilde{\mathbf{I}}(\tau, \hat{\mathbf{q}}) + \frac{1}{\langle C_{\text{ext}} \rangle_\xi} \int_{4\pi} \mathrm{d}\hat{\mathbf{n}}' \langle \mathbf{Z}(\hat{\mathbf{q}}, \hat{\mathbf{q}}') \rangle_\xi \widetilde{\mathbf{I}}(\tau, \hat{\mathbf{q}}'), \tag{54}$$

where $d\tau = n_0 \langle C_{\text{ext}} \rangle_\xi \mathrm{d}z$ is the optical depth element, $\langle C_{\text{ext}} \rangle_\xi$ is the average extinction cross section per particle, and $u = -\cos\theta$ is the direction cosine. The z-axis of the laboratory right-handed coordinate system is assumed to be perpendicular to the plane boundaries of the medium and directed upwards.

The most important corollaries of the microphysical derivation of the RTE are the following [34].

- The derivation of the RTE does not need fundamental physical laws other than those already contained in the classical macroscopic electromagnetics. In particular, the ill-defined concepts of collective effects, elementary volume elements, incoherent light rays, and photons as localized particles of light have no relevance whatsoever to the transfer of electromagnetic radiation in discrete random media.
- The RTE is derived by keeping only one class of wavelet pairs illustrated by Figs. 13(b) and 16(f). The effect of unconnected particles is reduced to attenuation and dichroism.
- In the context of the RT theory, the scattering properties of particles are specified in terms of the extinction and phase matrices rather than in terms of the scattering dyadic or the scattering amplitude matrix.
- Each particle with its individual extinction and phase matrices is effectively replaced with an average particle having the extinction and phase matrices obtained by averaging over all particle states.
- In the framework of the exact FLEs, the source of multiple scattering is the constant-amplitude incident field, Eq. (28b). In the framework of the approximate RTT, this role is effectively assumed by the exponentially attenuated coherent (or "unscattered") part of the specific intensity column vector $\mathbf{I}_{\text{c}}$ described by Eq. (52).
- Averaging over all particle positions makes $\mathbf{I}_{\text{c}}$ and $\widetilde{\mathbf{I}}_{\text{d}}$ continuous functions of the position vector of the observation point $\mathbf{r}$ and also makes $\widetilde{\mathbf{I}}_{\text{d}}$ a continuous function of the propagation direction $\hat{\mathbf{q}}$.
- For the same reason, $\widetilde{\mathbf{I}}$ differs from the Stokes column vector of a transverse electromagnetic wave, $\mathbf{I}$, in that it has the dimension of monochromatic radiance, $\mathrm{Wm^{-2}sr^{-1}}$, rather than the

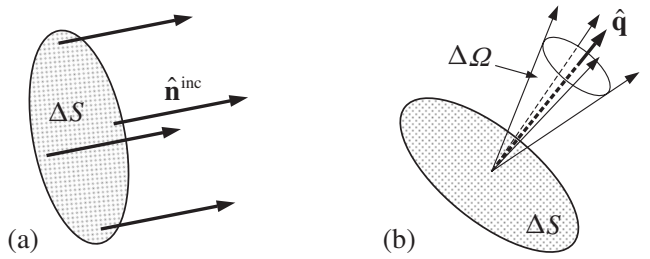

Figure 18. Physical meaning of (a) coherent intensity and (b) specific intensity.

dimension of monochromatic energy flux, Wm^{-2}.

- The RTE is an inherently vector equation. The frequently used scalar version of the RTE is obtained by artificially replacing the specific intensity vector by its first element (i.e., the specific intensity) and the normalized phase matrix by its (1, 1) element (i.e., the phase function). As such, the scalar approximation has no compelling physical justification besides being easier to solve and providing acceptable accuracy in many cases.
- The RTE remains valid if the incident light is a parallel quasi-monochromatic beam.

The integral form of the RTE can be used to clarify the physical meaning of the coherent Stokes column vector $\mathbf{I}_{\text{c}}$ and the diffuse specific intensity column vector $\widetilde{\mathbf{I}}_{\text{d}}$. The fundamental difference between these quantities is that the former describes a monodirectional whereas the latter describes an uncollimated flow of electromagnetic energy. In particular, the first element of the coherent Stokes column vector, i.e., the coherent intensity $I_{\text{c}}(\mathbf{r})$, is the electromagnetic power per unit area of a small surface element perpendicular to the incidence direction $\mathbf{n}^{\text{inc}}$, whereas the first element of the diffuse specific intensity column vector, i.e., the diffuse specific intensity $\widetilde{I}_{\text{d}}(\mathbf{r}, \hat{\mathbf{q}})$, is the electromagnetic power per unit area of a small surface element perpendicular to $\hat{\mathbf{q}}$ per one steradian of a small solid angle centered around $\hat{\mathbf{q}}$ (Fig. 18).

This interpretation of $\mathbf{I}_{\text{c}}(\mathbf{r})$ and $\widetilde{\mathbf{I}}_{\text{d}}(\mathbf{r}, \hat{\mathbf{q}})$ implies that both quantities can be measured by appropriately placed and oriented detectors of electromagnetic energy. The fact that the specific intensity column vector can be both computed theoretically by solving the RTE and measured with a suitable optical device explains the practical usefulness of the RT theory in countless applications in various branches of science and engineering.

Since the microphysical derivation of the RTE involves statistical averaging over particle states and positions, neither the coherent Stokes column vector nor the diffuse specific intensity column vector characterize the instantaneous distribution of the radiation field inside the scattering medium. Instead, they characterize the directional flow of electromagnetic radiation averaged over a sufficiently long period of time. The minimal averaging time necessary to ensure ergodicity may be different for different scattering systems, but the following is always true: the longer the averaging time the more accurate the theoretical prediction based on the RTE. Accumulating a signal over an extended period of time is often used to improve the accuracy of a measurement by reducing the effect of random noise. However, the situation with the RT theory is fundamentally different in that averaging the signal over an extended period of time is necessary to ensure the very applicability of the RTE.

Although the microphysical derivation of the RTE rests on several fundamental premises discussed above, most of them appear to be quite realistic in a great variety of applications. However, the assumptions of ergodicity and spatial uniformity deserve a separate analysis.

The meaning of the assumption or ergodicity is illustrated in Fig. 19. The detector of electromagnetic energy has an angular aperture small enough to resolve the angular variability of the radiation field (e.g., ~1°) and a finite acceptance area ΔS. Both define the part of the scattering volume V bounded schematically by the dotted lines in Fig. 19; this part will be called the

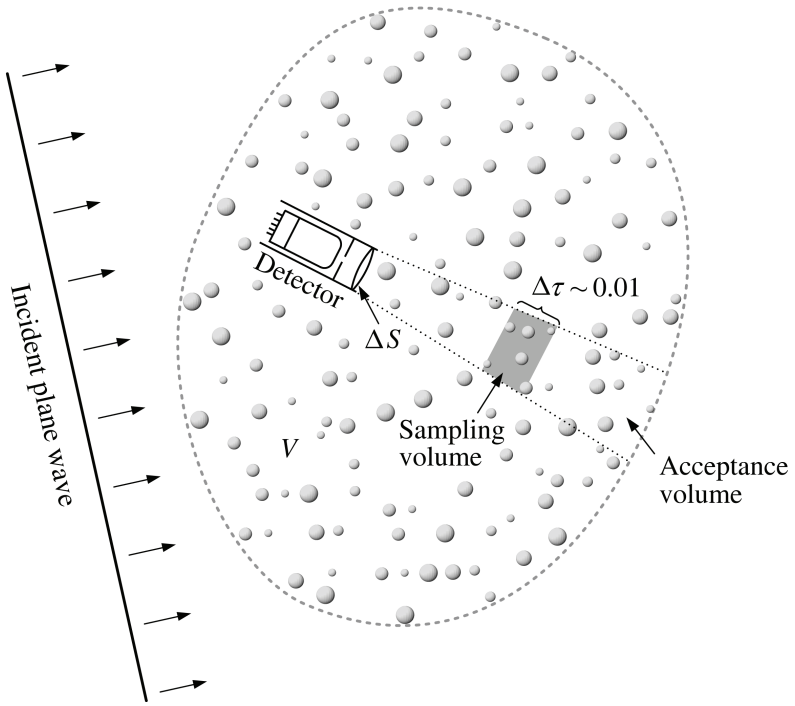

Figure 19. Practical meaning of the assumptions of ergodicity and uniformity.

acceptance volume. According to the integral form of the RTE, all energy recorded by the detector comes directly from the particles contained in the acceptance volume. The energy exciting each particle can be either the (attenuated) incident light or the light scattered by the other particles. The light scattered by a particle from the acceptance volume towards the detector can be attenuated by other particles located closer to the detector.

Let us assume that the detector accumulates the signal over a time interval Δt and subdivide the acceptance volume into a number of sampling volumes such that their optical thickness $\Delta\tau$ along the line of sight of the detector is very small (~0.01). One of these sampling volumes is shown schematically in Fig. 19. Obviously, the contribution of a particle to the detector signal is essentially independent of the specific particle position in the sampling volume. Therefore, the *strict* meaning of the assumptions of ergodicity and statistical uniformity of particle and inclusion positions within the scattering volume V is that each particle visits each sampling volume during the measurement interval Δt.

In reality, the scattering volume V contains many particles of the same type. Therefore, the *practical* meaning of ergodicity and uniformity is that particles of each type visit each sampling volume during the measurement interval Δt a number of times statistically representative of the total number of such particles in the entire scattering volume.

13. COEHERNT BACKSCATTERING

Consider again a scattering object in the form of a large group of discrete, randomly and sparsely distributed particles, Fig. 20. The object is illuminated by a plane electromagnetic wave propagating in the direction of a unit vector $\hat{\mathbf{n}}^{\text{inc}}$. The reader may recall that the RTE is derived by neglecting all diagrams with crossing connectors in the diagrammatic representation of the coherency dyadic. Following the line of reasoning outlined in the previous section, one may indeed conclude that upon statistical averaging the contribution of all the diagrams of the type illustrated in Fig. 21 must vanish at near-field observation points located either inside the object (observation point 1 in Fig. 20) or outside the object (observation point 2).

However, there is an exception corresponding to the situation when the observation point is in

Figure 20. Scattering of a plane electromagnetic wave by a volume of sparse, discrete random medium.

the far-field zone of the scattering object and is located within its "back-shadow" (observation point 3). Then the class of diagrams illustrated by Fig. 13(a) and panels (c)–(e) in Fig. 21 gives a nonzero contribution that causes CB. These diagrams are called maximally crossed since they can be drawn in such a way that all connectors cross at one point.

The expression for the cumulative contribution of all maximally crossed (or cyclical) diagrams to the coherency dyadic at an observation point can be derived using the diagrammatic technique introduced in the preceding section. The final result can be summarized by the diagrammatic expression shown in Fig. 22. The symbol Σ has the usual meaning and denotes both the summation over all appropriate particles and the statistical averaging over the particle states and positions, whereas the double lines account for the effect of exponential attenuation and, possibly, dichroism. It is very instructive to compare Fig. 22 with Fig. 17 since this comparison reveals quite vividly the morphological difference between the participating diagrams. The total coherency dyadic is now approximated by the following expression:

$$\ddot{C} \approx \ddot{C}_{\text{L}} + \ddot{C}_{\text{C}}. \tag{55}$$

The inclusion of the cyclical diagrams makes the computation of the coherency dyadic much more involved and limits the range of problems that can be solved accurately. In particular, no closed-form equation similar to the RTE has been derived to describe the CB contribution to the specific coherency dyadic, $\ddot{\Sigma}_{\text{C}}(\mathbf{r}, \hat{\mathbf{q}})$. However, the reciprocal nature of each single-scattering event leads to an interesting exact result: the characteristics of the CB effect at the exact backscattering direction can be rigorously expressed in terms of the solution of the RTE. This result as well as other relevant theoretical and numerical approaches to the problem of CB are reviewed in [34, 55, 56].

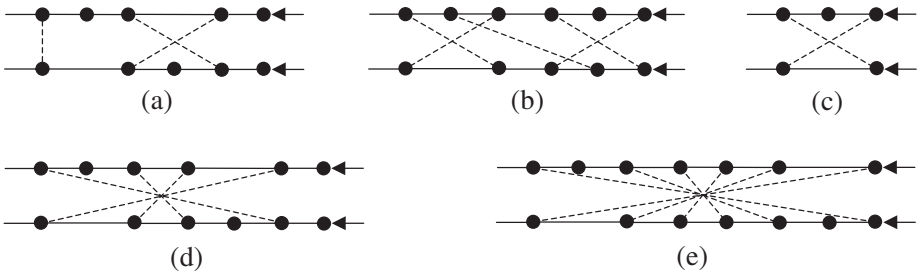

Figure 21. Diagrams with crossing connectors.

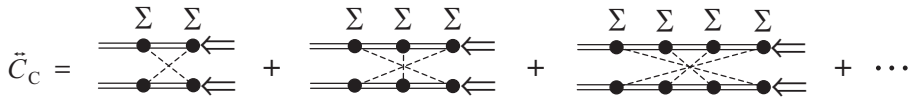

Figure 22. The cyclical part of the coherency dyadic.

CB is an expressly far-field effect. In reality, however, CB can be observed at distances shorter than those dictated by Eq. (14). Specifically, the distance d from the scattering medium to the observation point must satisfy the following inequality [34]:

$$d \gg \tfrac{1}{2} k_1 L^2, \qquad L = \min(D, l_{\mathrm{tr}}), \tag{56}$$

where D is the maximal linear dimension of the scattering volume and l_{tr} is the so-called transport mean free path. If the scattering medium is composed of nonabsorbing, wavelength-sized or larger particles and is such that $D \geq l_{\mathrm{tr}}$ then the requirement (56) can be rather demanding.

14. FORWARD-SCATTERING INTERFERENCE

Similarly to CB, the forward-scattering interference discussed in Section 11.3 is an expressly far-field scattering effect and as such is not accounted for by the RTE. Indeed, it can be readily shown that the contribution of the diagrams of the type shown in Fig. 16(b) evaluated at a near-field observation point does not vanish only when both particles are positioned along the same straight line parallel to the incidence direction and going through the observation point. This non-vanishing contribution is ultimately included in the exponentially attenuated coherent Stokes column vector $\mathbf{I}_{\mathrm{c}}$.

In order to observe the forward-scattering interference effect directly, the observation point must be located in the far-field zone, i.e., at a distance r from the scattering volume satisfying the inequalities (12)–(14). This factor makes the RTE a rather robust approximation. To appreciate this point, one can apply Eq. (14) to a small cloud of water droplets with a typical dimension of 100 m assuming that the incident wavelength is 500 nm. Simple arithmetic then yields $r \gg 3 \times 10^{10}$ m.

ACKNOWLEDGEMENTS

The author thanks Joop Hovenier, Dan Mackowsky, Victor Tishkovets, and Gorden Videen for numerous illuminating discussions. This research was supported by the NASA Radiation Sciences Program managed by Hal Maring.

REFERENCES

1. Lommel, E., Die Photometrie der diffusen Zurückwerfung, *Sitzber. Acad. Wissensch. München*, Vol. 17, pp 95–124, 1887.
2. Chwolson, O., Grundzüge einer mathematischen Theorie der inneren Diffusion des Lichtes, *Bull. l'Acad. Impériale Sci. St. Pétersbourg*, Vol. 33, pp 221–256, 1889.
3. Chandrasekhar, S., *Radiative Transfer*, Oxford University Press, Oxford, 1950.
4. Sobolev, V. V., *Light Scattering in Planetary Atmospheres*, Pergamon Press, Oxford, 1975.
5. van de Hulst, H. C., *Multiple Light Scattering. Tables, Formulas, and Applications*, Vols. 1 and 2, Academic Press, San Diego, California, 1980.
6. Viskanta, R., and Mengüç, M. P., Radiation Heat Transfer in Combustion Systems, *Progr. Energy Combust. Sci.*, Vol. 13, pp 97–160, 1987.
7. Goody, R. M., and Yung, Y. L., *Atmospheric Radiation: Theoretical Basis*, Oxford University Press, Oxford, 1989.
8. Lenoble, J., *Atmospheric Radiative Transfer*, A. Deepak Publishing, Hampton, Virginia, 1993.
9. Fung, A. K., *Microwave Scattering and Emission Models and Their Applications*, Artech House, Boston, Massachusetts, 1994.
10. Yanovitskij, E. G., *Light Scattering in Inhomogeneous Atmospheres*, Springer, Berlin, 1997.

11. Thomas, G. E., and Stamnes, K., *Radiative Transfer in the Atmosphere and Ocean*, Cambridge University Press, Cambridge, 1999.
12. Tsang, L., Kong, J. A., and Ding, K.-H., *Scattering of Electromagnetic Waves: Theories and* Applications, Wiley, New York, 2000.
13. Tuchin, V. V., ed., *Handbook of Optical Biomedical Diagnostic*, SPIE Press, Bellingham, Washington, 2002.
14. Siegel, R., and Howell, J. R., *Thermal Radiation Heat Transfer*, Taylor & Francis, New York, 2002.
15. Liou, K. N., *An Introduction to Atmospheric Radiation*, Academic Press, San Diego, California, 2002.
16. Modest, M. *Radiative Heat Transfer*, Academic Press, San Diego, California, 2003.
17. Hovenier, J. W., van der Mee, C., and Domke, H., *Transfer of Polarized Light in Planetary Atmospheres—Basic Concepts and Practical Methods*, Springer, Berlin, 2004.
18. Marshak, A., and Davis, A. B., eds., 3D *Radiative Transfer in Cloudy Atmospheres*, Springer, Berlin, 2005.
19. Bohren, C. F., and Clothiaux, E. E., *Fundamentals of Atmospheric Radiation*, Wiley-VCH, Weinheim, Germany, 2006.
20. Power, E. A., *Introductory Quantum Electrodynamics*, Longmans, London, 1964.
21. Akhiezer, A. I., and Berestetskii, V. B., *Quantum Electrodynamics*, Wiley, New York, 1965.
22. Mandel, L., and Wolf, E., *Optical Coherence and Quantum Optics*, Cambridge University Press, Cambridge, 1995.
23. Meystre, P., and Sargent, M., III, *Elements of Quantum Optics*, Springer, Berlin, 1999.
24. Kidd, R., Ardini, J., and Anton, A., Evolution of the Modern Photon, *Am. J. Phys*., Vol. 57, pp 27–35, 1989.
25. Lamb, W. E., Jr., Anti-Photon, *Appl. Phys. B*, Vol. 60, pp 77–84, 1995.
26. Wolf, E., Coherence and Radiometry, *J. Opt. Soc. Am*., Vol. 68, pp 6–17, 1978
27. Schiff, L. I., *Quantum Mechanics*, McGraw-Hill, New York, 1968.
28. Fearn, H., and Lamb, W. E., Jr., Corrections to the Golden Rule, *Phys. Rev. A*, Vol. 43, pp 2124–2128, 1991.
29. Townes, C. H., Ideas and Stumbling Blocks in Quantum Electronics, *IEEE J. Quant. Electron*., Vol. 20, pp 547–550, 1984.
30. Apresyan, L. A., and Kravtsov, Yu. A., *Radiation Transfer. Statistical and Wave Aspects*, Gordon and Breach, Basel, 1996.
31. Tsang, L., and Kong, J. A., *Scattering of Electromagnetic Waves: Advanced Topics*, Wiley, New York, 2001.
32. Mishchenko, M. I., Vector Radiative Transfer Equation for Arbitrarily Shaped and Arbitrarily Oriented Particles: A Microphysical Derivation from Statistical Electromagnetics, *Appl. Opt.*, Vol. 41, pp 7114–7134, 2002.
33. Mishchenko, M. I., Microphysical Approach to Polarized Radiative Transfer: Extension to the Case of an External Observation Point, *Appl. Opt.*, Vol. 42, pp 4963–4967, 2003.
34. Mishchenko, M. I., Travis, L. D., and Lacis, A. A., *Multiple Scattering of Light by Particles: Radiative Transfer and Coherent Backscattering*, Cambridge University Press, Cambridge, 2006.
35. Stratton, J. A., *Electromagnetic Theory*, McGraw-Hill, New York, 1941.
36. Jackson, J. D., *Classical Electrodynamics*, Wiley, New York, 1999.
37. Saxon, D. S., Lectures on the Scattering of Light, Scientific Report No. 9, Department of Meteorology, University of California at Los Angeles, 1955.
38. Mishchenko, M. I., Travis, L. D., and Lacis, A. A., *Scattering, Absorption, and Emission of Light by Small Particles*, Cambridge University Press, Cambridge, 2002 (available in the .pdf format at http://www.giss.nasa.gov/~crmim/books.html).
39. Tsang, L., Kong, J. A., and Shin, R. T., *Theory of Microwave Remote Sensing*, Wiley, New York, 1985.
40. Newton, R. G., *Scattering Theory of Waves and Particles*, Springer, New York, 1982.
41. Mishchenko, M. I., Hovenier, J. W., and Travis, L. D., eds., *Light Scattering by Nonspherical Particles: Theory, Measurements, and Applications*, Academic Press, San Diego, California, 2000.
42. Kahnert, F. M., Numerical Methods in Electromagnetic Scattering Theory, *J. Quant. Spectrosc. Radiat. Transfer*, Vol. 79–80, pp 775–824, 2003.
43. Babenko, V. A., Astafyeva, L. G., and Kuzmin, V. N., *Electromagnetic Scattering in Disperse Media: Inhomogeneous and Anisotropic Particles*, Springer, Berlin, 2003.
44. Doicu, A., Wriedt, T., and Eremin, Y. A., *Light Scattering by Systems of Particles*, Springer, Berlin,

2006.
45. Stokes, G. G., On the Composition and Resolution of Streams of Polarized Light from Different Sources, *Trans. Cambridge Philos. Soc.*, Vol. 9, pp 399–416, 1852.
46. Fuller, K., and Mackowski, D. W., Electromagnetic Scattering by Compounded Spherical Particles, in Mishchenko, M. I., Hovenier, J. W., and Travis, L. D., eds., *Light Scattering by Nonspherical Particles, Theory, Measurements, and Applications*, pp 225–272, Academic Press, San Diego, California, 2000.
47. Borghese, F., Denti, P., and Saija, R., *Scattering from Model Nonspherical Particles: Theory and Applications to Environmental Physics*, Springer, Berlin, 2007.
48. Martin, P. A., *Multiple Scattering: Interaction of Time-Harmonic Waves with* N *Obstacles*, Cambridge University Press, Cambridge, 2006.
49. Mishchenko, M. I., Liu, L., Mackowski, D. W., Cairns, B., and Videen, G., Multiple Scattering by Random Particulate Media: Exact 3D Results, *Opt. Express*, in press, 2007.
50. Berne, B. J., and Pecora, R., *Dynamic Light Scattering with Applications to Chemistry, Biology, and Physics*, Wiley, New York, 1976.
51. Brown, W., ed., *Dynamic Light Scattering*, Clarendon Press, Oxford, 1993.
52. Mackowski, D. W., A Simplified Model to Predict the Effects of Aggregation on the Absorption Properties of Soot Particles, *J. Quant. Spectrosc. Radiat. Transfer*, Vol. 100, pp 237–249, 2006.
53. Mackowski, D. W., and Mishchenko, M. I., Calculation of the *T* Matrix and the Scattering Matrix for Ensembles of Spheres, *J. Opt. Soc. Am. A*, Vol. 13, pp 2266–2278, 1996.
54. Twersky, V., On Propagation in Random Media of Discrete Scatterers, *Proc. Symp. Appl. Math.*, Vol. 16, 84–116, 1964.
55. Kuz'min, V. L., and Romanov, V. P., Coherent Phenomena in Light Scattering from Disordered Systems, *Phys.–Uspekhi*, Vol. 39, pp 231–260, 1996.
56. van Rossum, M. C. W., and Nieuwenhuizen, T. M., Multiple Scattering of Classical Waves: Microscopy, Mesoscopy, and Diffusion, *Rev. Mod. Phys*., Vol. 71, pp 313–371, 1999.